Ozone Data Assimilation with GEOS-Chem: a Comparison Between 3D-Var, 4D-Var, and Suboptimal Kalman Filter Approaches

K. Singh[1], A. Sandu[1], K. W. Bowman[2], M. Parrington[3], D. B. A. Jones[4], and M. Lee[2]

Corresponding author: A. Sandu, Computational Science Laboratory, Department of Computer Science, Virginia Polytechnic Institute and State University, 2202 Kraft Drive, Blacksburg, VA 24060, USA. E-mail: sandu@cs.vt.edu. Tel: 540-231-2193. Fax: 540-231-9218.

[1]Computational Science Laboratory, Department of Computer Science, Virginia Polytechnic Institute and State University, 2202 Kraft Drive, Blacksburg, VA 24060, USA

[2]Jet Propulsion Laboratory, 4800 Oak Grove Drive, Pasadena, CA 91109, USA

[3]School of GeoSciences, University of Edinburgh, Edinburgh, UK

[4]Department of Physics, University of Toronto, ON M5S 1A7, Canada

Abstract. Chemistry transport models determine the evolving chemical state of the atmosphere by solving fundamental equations that govern physical and chemical transformations subject to initial conditions of the atmospheric state and surface boundary conditions, e.g., surface emissions. The development of data assimilation techniques synthesize model predictions with measurements in a rigorous mathematical framework that provides observational constraints on these conditions.

Two families of data assimilation methods are currently widely used: variational and Kalman filter (KF). The variational approach is based on control theory and formulates data assimilation as a minimization problem of a cost functional that measures the model-observations mismatch. The Kalman filter approach is rooted in statistical estimation theory and provides analysis covariance together with the best state estimate. Suboptimal Kalman filters employ different approximations of the covariances in order to make computations feasible with large models. Each family of methods have both merits and drawbacks.

This paper compares several data assimilation methods used for global chemical data assimilation. Specifically, we evaluate data assimilation approaches for improving estimates of the summertime global tropospheric ozone distribution in August 2006 based on ozone observations from the NASA Tropospheric Emission Spectrometer and the GEOS-Chem chemistry transport model. The resulting analyses are compared against independent ozonesonde measurements to assess the effectiveness of each

assimilation method. All assimilation methods provide notable improvements over the free model simulations, which differ from ozonesonde measurements by about 20% (below 200 hPa). Four dimensional variational data assimilation with window lengths between five days and two weeks is the most accurate method, with mean differences between analysis profiles and ozonesonde measurements of 1-5%. Two sequential assimilation approaches (three dimensional variational and suboptimal KF), although derived from different theoretical considerations, provide similar ozone estimates, with relative differences of 5-10% between the analyses and ozonesonde measurements.

Adjoint sensitivity analysis techniques are used to explore the role of uncertainties in ozone precursors and their emissions on the distribution of tropospheric ozone. A novel technique is introduced that projects 3D-Variational increments back to an equivalent initial condition, which facilitates comparison with 4D variational techniques

1. Introduction

Understanding the distribution of tropospheric ozone is one of the principal scientific challenges in global atmospheric chemistry, e.g., Jacob [1999]. Ozone is an integral constituent of the troposphere that plays a significant role in determining chemical and radiative state of the atmosphere. Ozone in stratosphere absorbs UV radiation, which is harmful to human health. In upper troposphere, ozone is a greenhouse gas through absorption of upwelling long wave radiation. In the mid-troposphere, ozone is a precursor to OH radicals which moderate pollution levels. At the surface, ozone is a pollutant causing respiratory problems and affecting crop yields.

Numerous studies have attempted to quantify the distribution of tropospheric ozone through chemical transport models. Findings from these studies vary significantly due to the strong variability in ozone lifetimes and uncertainties in determining the amount of ozone lost through dry deposition, entered through upper troposphere-stratosphere exchanges, or evolved due to chemical reactions of trace gas and emission precursors. Ozone lifetime varies from a few minutes at the surface, to a few days in the lower troposphere, to months in the upper troposphere. In such situations, it is important to validate the accuracy of model predictions against observed state of the atmosphere. Studies of variations in tropospheric ozone have been conducted through ozonesonde measurements, surface measurements [Logan, 1994, 1999; Tarasick et al., 2005; Oltmans et al., 2006], and satellite observations [Munro et al., 1998; Tellmann et al., 2004].

Chemical data assimilation is a process of optimally combining imperfect observations with imperfect model simulations to produce a better estimate of the chemical state of the atmosphere and its boundary conditions [Carmichael et al., 2008]. Considerable experience with data assimilation has been accumulated in the field of numerical weather prediction [Daley, 1991; Courtier et al., 1998; Rabier et al., 2000; Kalnay, 2002; Navon, 2009; Lahoz and Errera, 2010]. In this work, we focus on atmospheric constituent data assimilation. Chemical data assimilation poses specific challenges related to the multiphysics nature of the system, the stiffness of chemical kinetic equations, the sparseness of chemical observations, and the uncertainty in the levels of anthropogenic and natural pollutants emitted into the atmosphere. Throughout this paper we will refer to model results as model predictions or model forecasts even when a past period is simulated.

Previous studies have employed various approaches to assimilating observations of trace gases for improved tropospheric chemistry representations. Data assimilation has been used to improve initial conditions, boundary values (emissions), and has resulted in improved air quality forecasts. Early work in chemical data assimilation using variational techniques has been reported in Fisher and Lary [1995]; Elbern et al. [1997]; Khattatov et al. [1999]; Errera and Fonteyn [2001]; Elbern and Schmidt [2001]. Since then there is a growing body of literature with applications of 3D-Var and 4D-Var chemical data assimilations. The base concepts of variational approach to chemical data assimilation, and the construction of adjoint chemical transport models are discussed in detail in Sandu et al. [2005a]; Hakami et al. [2007]; Henze et al. [2007]; Carmichael et al. [2008]. 3D-Var was first used by Derber et al. [1991]; Parrish

and Derber [1992] and later applied by most of the meteorological centers [Courtier et al., 1998; Cohn et al., 1998; Gauthier et al., 1999a]. A study on ozone improvement using 3D-Var assimilation is presented in Bei et al. [2008]. Adjustment of gas phase chemical tracer initial conditions has been studied in Chai et al. [2007]; Sandu et al. [2005b]; Tang et al. [2004]; Zhang et al. [2008]. Adjustment of pollutant emissions through 4D-Var chemical data assimilation has been discussed in Chai et al. [2009]. Data assimilation studies involving particle measurements to improve aerosol fields have been discussed in Hakami et al. [2005]; Sandu et al. [2005b]; Henze et al. [2004, 2009]. Suboptimal Kalman filters have been employed successfully for chemical data assimilation [Khattatov et al., 2000; Menard et al., 2000; Lamarque et al., 2002; Liao et al., 2006; Segers et al., 2005; Clark et al., 2006; Pierce et al., 2007; Parrington et al., 2009]. The use of the ensemble Kalman filter (EnKF) [Evensen, 1994] in chemical data assimilation has been studied in Constantinescu et al. [2007a, b, c].

Different approaches to data assimilation are rooted in different theories (control, statistical estimation), have different implementations and computational costs, and yield different performances on large scale problems of practical interest. A discussion on relationship between optimality of variational data assimilation and Kalman filter is presented in Li and Navon [2001]. Houtekamer [2005] compared the quality of background statistics in 3D-Var and EnKF using radiance observations from satellite, while, Laroche et al. [2005] compared the characteristics of 3D-Var and 4D-Var introduced in the operational suite of the Canadian Meteorological Center (CMC). Constantinescu et al. [2007c] and Wu et al. [2008] compare the performances of EnKF with 4D-Var for chemical transport models on a regional scale using ground-level

ozone measurements, while, Geer et al. [2006] provide an intercomparison of stratospheric ozone estimates obtained through 3D-Var, 4D-Var, and Kalman filter assimilation systems for both chemical transport and global circulation models as part of the Assimilation of ENVISAT Data (ASSET) project. The comparison between techniques in Wu et al. [2008] is done in the context of regional assimilation and using surface network data.

The Tropospheric Emission Spectrometer (TES) [Beer et al., 2001] is the first dedicated infrared instrument from which information of the global and vertical distribution of tropospheric ozone can be retrieved. Parrington et al. [2009] reported assimilation of vertical profiles of ozone from TES into the GEOS-Chem using suboptimal Kalman filter while Pierce et al. [2009] used TES and OMI in conjunction with a simple univariate filtering approach to investigate the impact of distant sources on air quality in Dallas and Houston. We have developed 3D-Var and 4D-Var data assimilation capabilities for GEOS-Chem v7. The goal of this paper is to provide the first direct comparison of global tropospheric ozone distribution estimated through 3D-Var, 4D-Var and suboptimal KF assimilation systems showcasing the potential of TES profile retrievals. The assessment of analyses generated through different assimilation systems is on the similar lines of Geer et al. [2006]; Parrington et al. [2009].

This paper is structured as follows: Section 2 provides the mathematical overview of how observations are integrated into the model in different data assimilation systems. Section 5.2 discusses characteristics of background error covariance matrices used in this study. Section 3 provides a brief overview of the global chemical transport model (GEOS-Chem) and its adjoint development. A description of the TES instrument,

its observation operator and profile retrieval formulation is provided in Section 4. Section 6 details the experimental settings, computational costs and assessment of tropospheric ozone estimates through different assimilation systems. Summary and points of future work are discussed in Section 7.

2. Chemical data assimilation

Variational methods solve the data assimilation problem in an optimal control framework [Sasaki, 1958; Le Dimet and Talagrand, 1986; Courtier and Talagrand, 1987; Lions, 1971]. Specifically, they attempt to find the control variable values (e.g., initial conditions) that minimize the discrepancy between the model forecast and observations subject to the governing dynamic equations, taking into account the error covariances of the forecast and the observations. In contrast, statistical estimation methods (generically known as Kalman filters/smoothers) solve the data assimilation problem in a Bayesian framework by combining probability densities of errors from different sources [Khattatov et al., 2000; Menard et al., 2000; Lamarque et al., 2002; Segers et al., 2005; Clark et al., 2006; Pierce et al., 2007; Parrington et al., 2009; Constantinescu et al., 2007b, c]. In the following discussion, for simplicity of presentation, we focus on discrete models (in time and space) where the initial conditions are the control variables.

Data assimilation provides best estimates of the state of the atmosphere by combining the following three sources of information.

1. The apriori, or background state $\mathbf{x}^b$ represents the best estimate of the true state $\mathbf{x}^t$ available before any measurements are taken. This estimate is assumed unbiased, and the random background (estimation) errors ε^b are typically assumed to have a

normal probability density with a background error covariance matrix **B**

$$\varepsilon^b = \mathbf{x}^b - \mathbf{x}^t \in \mathcal{N}(\mathbf{0}, \mathbf{B}). \tag{1}$$

2. The model encapsulates our knowledge about physical and chemical laws that govern the evolution of the system. The model evolves an initial state $\mathbf{x}_0 \in \mathbb{R}^n$ at the initial time t_0 to future state values $\mathbf{x}_i \in \mathbb{R}^n$ at future times t_i,

$$\mathbf{x}_i = \mathcal{M}_{t_0 \to t_i}(\mathbf{x}_0). \tag{2}$$

The size of the state space in realistic chemical transport models is very large. For example, a GEOS-Chem simulation at the $2^\circ \times 2.5^\circ$ horizontal resolution has $n \in \mathcal{O}(10^8)$ variables.

3. Observations $\mathbf{y}_i \in \mathbb{R}^m$ of the state are taken at times t_i, $1 = 1, \cdots, N$

$$\mathbf{y}_i = \mathcal{H}(\mathbf{x}_i) + \varepsilon_i^{\text{obs}}. \tag{3}$$

The observation operator $\mathcal{H}$ maps the model state vector onto the observation space. In many practical situations $\mathcal{H}$ is a highly nonlinear mapping , e.g., satellite radiance operators.

The observations are characterized by measurement and representativeness errors $\varepsilon_i^{\text{obs}}$. The observation errors at each time are assumed to be independent of background errors, and independent of the observation errors at other times. They are typically assumed to have a normal distribution with mean zero and covariance $\mathbf{R}_i$,

$$\varepsilon_i^{\text{obs}} \in \mathcal{N}(\mathbf{0}, \mathbf{R}_i). \tag{4}$$

Based on these three sources of information data assimilation computes the posterior estimate $\mathbf{x}^a$ of the true state; $\mathbf{x}^a$ is called the "analysis" state.

2.1. Three dimensional variational (3D-Var) data assimilation

In the 3D-Var data assimilation the observations (3) are considered successively at times $t_1, \cdots, t_N$. The background state (i.e., the best state estimate at time t_i) is given by the model forecast, starting from the previous analysis (i.e., best estimate at time t_{i-1}):

$$\mathbf{x}_i^b = \mathcal{M}_{t_{i-1} \to t_i} \left(\mathbf{x}_{i-1}^a \right) .$$

The discrepancy between the model state $\mathbf{x}_i$ and observations at time t_i, together with the departure of the state from the model forecast $\mathbf{x}_i^b$, are measured by the 3D-Var cost function:

$$\mathcal{J}(\mathbf{x}_i) = \frac{1}{2} \left(\mathbf{x}_i - \mathbf{x}_i^b \right)^T \mathbf{B}_i^{-1} \left(\mathbf{x}_i - \mathbf{x}_i^b \right) + \frac{1}{2} \left(\mathcal{H}(\mathbf{x}_i) - \mathbf{y}_i \right)^T \mathbf{R}_i^{-1} \left(\mathcal{H}(\mathbf{x}_i) - \mathbf{y}_i \right) \tag{5}$$

The 3D-Var analysis is computed as the state which minimizes (5)

$$\mathbf{x}_i^a = \arg\min \mathcal{J} \left(\mathbf{x}_i \right) . \tag{6}$$

Typically a gradient-based numerical optimization procedure is employed to solve (6). The gradient $\nabla \mathcal{J}$ of the cost function (5) is

$$\nabla \mathcal{J} \left(\mathbf{x}_i \right) = \mathbf{B}_i^{-1} \left(\mathbf{x}_i - \mathbf{x}_i^b \right) + \mathbf{H}_i^T \mathbf{R}_i^{-1} \left(\mathcal{H}(\mathbf{x}_i) - \mathbf{y}_i \right) \tag{7}$$

Note that the gradient requires to computation of the linearized observation operator $\mathbf{H}_i = \mathcal{H}'(\mathbf{x}_i)$ about the current state $\mathbf{x}_i$.

Preconditioning is often used to improve convergence of the numerical optimization problem (6). A change of variables is performed by shifting the state and scaling it with the square root of covariance:

$$\widehat{\mathbf{x}}_i = \mathbf{B}_i^{1/2} \left(\mathbf{x}_i - \mathbf{x}_i^b \right) , \tag{8}$$

and carrying out the optimization with the new variables $\widehat{\mathbf{x}}_i$.

2.2. Four dimensional variational (4D-Var) data assimilation

In strongly-constrained 4D-Var data assimilation all observations (3) at all times $t_1, \cdots, t_N$ are simultaneously considered. The control parameters are the initial conditions $\mathbf{x}_0$; they uniquely determine the state of the system at all future times via the model equation (2).

The discrepancy between model predictions and observations at all future times $t_1, \cdots, t_N$, together with the departure of the initial state from the background state, are measured by the 4D-Var cost function:

$$\mathcal{J}\left(\mathbf{x}_0\right) = \frac{1}{2}\left(\mathbf{x}_0 - \mathbf{x}_0^b\right)^T \mathbf{B}_0^{-1} \left(\mathbf{x}_0 - \mathbf{x}_0^b\right) + \frac{1}{2}\sum_{i=1}^{N}\left(\mathcal{H}(\mathbf{x}_i) - \mathbf{y}_i\right)^T \mathbf{R}_i^{-1} \left(\mathcal{H}(\mathbf{x}_i) - \mathbf{y}_i\right) \quad (9)$$

Note that the departure of the initial conditions from the background is weighted by the inverse background covariance matrix, $\mathbf{B}^{-1}$, while the differences between the model predictions $\mathcal{H}(\mathbf{x}_i)$ and observations $\mathbf{y}_i$ are weighted by the inverse observation error covariances, $\mathbf{R}_i^{-1}$.

The 4D-Var analysis is computed as the initial condition which minimizes (9) subject to the model equation constraints (2)

$$\mathbf{x}_0^a = \arg\min \mathcal{J}\left(\mathbf{x}_0\right) \quad \text{subject to} (2). \quad (10)$$

The model (2) propagates the optimal initial condition (9) forward in time to provide the analysis at future times, $\mathbf{x}_i^a = \mathcal{M}_{t_0 \to t_i}\left(\mathbf{x}_0^a\right)$.

The optimization problem (10) is solved numerically using a gradient-based technique. The gradient of (9) reads

$$\nabla J\left(\mathbf{x}_0\right) = \mathbf{B}_0^{-1}\left(\mathbf{x}_0 - \mathbf{x}_0^b\right) + \sum_{i=1}^{N}\left(\frac{\partial \mathbf{x}_i}{\partial \mathbf{x}_0}\right)^T \mathbf{H}_i^T \mathbf{R}_i^{-1}\left(\mathcal{H}(\mathbf{x}_i) - \mathbf{y}_i\right) \quad (11)$$

The 4D-Var gradient requires not only the linearized observation operator $\mathbf{H}_i$, but also the transposed derivative of future states with respect to the initial conditions. The 4D-Var gradient can be obtained effectively by forcing the adjoint model with observation increments, and running it backwards in time.

2.3. Suboptimal Kalman filter

The suboptimal Kalman filter is a sequential data assimilation approach [Khattatov et al., 2000] in which corrections in the concentration state vector are performed as soon as observations become available. Similar to 3D-Var, for every observation time t_i, this technique starts with the model forecast state ($\mathbf{x}_i^f$) and provides an expected analysis state ($\mathbf{x}_i^a$) that reduces the discrepancy between the model forecast and the observations $\mathbf{y}_i$. The analysis state vector is obtained as

$$\mathbf{x}_i^a = \mathbf{x}_i^f + \mathbf{K}_i \left(\mathbf{y}_i - \mathcal{H} \left(\mathbf{x}_i^f \right) \right) \tag{12}$$

where $\mathcal{H}$ is the observation operator defined in equation (3) and $\mathbf{y}$ the vector of observations at a given time. The Kalman gain matrix ($\mathbf{K}$) is defined as

$$\mathbf{K}_i = \mathbf{P}_i^f \mathbf{H}^{\mathrm{T}} \left(\mathbf{H}_i \, \mathbf{P}_i^f \, \mathbf{H}_i^{\mathrm{T}} + \mathbf{R}_i \right)^{-1} \tag{13}$$

where $\mathbf{P}_i^f$ is the forecast error covariance matrix, $\mathbf{R}_i$ is the observation error covariance matrix (4), and $\mathbf{H}_i = \mathcal{H}'(\mathbf{x}_i^f)$ is the linearized observation operator about the forecast state. If a diagonal or block-diagonal approximation of the error covariance matrix $\mathbf{P}^f$ is used in equation (13), the analysis state generated through equation (12) is suboptimal. A description of the structure of $\mathbf{P}^f$ is provided in Section 5.2.

At each observation time, along with the analysis state, the analysis error covariance matrix $\mathbf{P}_i^a$ is also calculated as

$$\mathbf{P}_i^a = (\mathbf{I} - \mathbf{K}_i \mathbf{H}_i)\ \mathbf{P}_i^f \tag{14}$$

where $\mathbf{I}$ is the identity matrix. There are multiple ways in which this analysis covariance matrix is made available to the next observation window. A simple approach is to keep the analysis covariance equal to the background covariance for the entire assimilation period [Parrington et al., 2009]. Here we build diagonal approximations to $\mathbf{P}_{i+1}^f$ by transporting variances (diagonal entries in $\mathbf{P}_i^a$) as passive tracers following Menard et al. [2000].

3. GEOS-Chem

In this paper we specifically consider GEOS-Chem (`http://geos-chem.org`), a global three-dimensional chemical transport model (CTM) driven by assimilated meteorological fields from Goddard Earth Observing System(GEOS-4) at the NASA Global Modeling and Assimilation Office (GMAO). It is being widely used by research groups world-wide for performing global atmospheric chemistry studies. The model along with comparison of model predictions with observations was first described in Bey et al. [2001]. GEOS-Chem accounts in detail for emissions from both natural and anthropogenic sources, for tropospheric chemistry, aerosol processes, long range transport of pollutants, troposphere-stratosphere exchanges, etc. Anthropogenic emissions are obtained from the Global Emissions Inventory Activity (GEIA) [Benkovitz et al., 1996] while lightning NOx source emissions are estimated using Price and Rind [1992], based on deep convective cloud top heights provided with the

GMAO meteorological fields. Biomass burning emissions are based on Duncan et al. [2003] while biofuel emissions are from Yevich and Logan [2003]. The meteorological fields have a horizontal resolution of 1° along latitude and 1.25° along longitude with 55 vertical levels, and a temporal resolution of 6 hrs (3 hrs for surface fields). We use GEOS-Chem v7-04-10. Subsequent model releases and references can be found at `http://geos-chem.org`.

The GEOS-Chem Adjoint system (`http://wiki.seas.harvard.edu/geos-chem/index.php/GEOS-Chem_Adjoint`) has been developed through a joint effort of groups at Virginia Tech, University of Colorado, Caltech, Jet Propulsion Laboratory, and Harvard [Henze et al., 2007; Singh et al., 2009a, b; Eller et al., 2009]. The system can perform adjoint sensitivity analysis and 4D-Var chemical data assimilation. Inverse modeling studies with GEOS-Chem-Adjoint are exemplified in Henze et al. [2009]; Kopacz et al. [2007]; Zhang et al. [2009].

4. Tropospheric Emission Spectrometer (TES)

TES [Beer et al., 2001], one of four science instruments aboard NASA's Aura satellite, measures top-of-the-atmosphere high resolution spectrally-resolved longwave radiation (`http://tes.jpl.nasa.gov`). Vertical profiles of chemical concentrations are inferred from these radiance measurements using an off-line inversion process [Bowman et al., 2006]. In this work we assimilate the retrieved ozone vertical profiles. Figure 1 shows the location of TES profiles for two days. Only TES profiles between 60°S- 60°N are considered because lower poleward thermal contrast pose difficulty in measurements leading to higher inaccuracies in the retrieved profiles.

A-priori information about the vertical concentration profile of the species of interest is needed to solve the retrieval inverse problem (the prior information does not come from the measurement). Let $\mathbf{x}^{\text{prior}}$ be the prior vertical ozone concentration profile (in volume mixing ratio units), and let $\mathbf{z}^{\text{prior}} = \log \mathbf{x}^{\text{prior}}$. Let $\mathbf{z}^{\text{true}}$ (=$\log \mathbf{x}^{\text{true}}$) be the "true" atmospheric profile.

The vertical ozone profile retrieval can be expressed according to the formula

$$\widehat{\mathbf{z}} = \mathbf{z}^{\text{prior}} + \mathbf{A}\left(\mathbf{z}^{\text{true}} - \mathbf{z}^{\text{prior}}\right) + \mathbf{G}\,\eta, \quad \widehat{\mathbf{x}} = \exp\left(\widehat{\mathbf{z}}\right). \tag{15}$$

Here $\mathbf{A}$ is the averaging kernel matrix, $\mathbf{G}$ is the gain matrix, and η is the spectral measurement error (assumed to have mean zero and covariance $\mathbf{S}_\eta$). More details can be found in Bowman et al. [2002]; Jones et al. [2003]; Worden et al. [2004].

The corresponding TES observation operator (3) is linear with respect to the logarithm of the concentrations, but nonlinear with respect to the concentration profile:

$$\mathcal{H}\left(\mathbf{x}\right) = \mathbf{z}^{\text{prior}} + \mathbf{A}\left(\log(\mathbf{L}\,\mathbf{x}) - \mathbf{z}^{\text{prior}}\right) \tag{16}$$

where $\mathbf{L}$ is an interpolation operator that transforms $\mathbf{x}$ from the GEOS-Chem N-level vertical grid to the TES profile retrieval P-level grid.

For this reason several chemical data assimilation studies based on TES retrieved profiles [Jones et al., 2003; Bowman et al., 2006; Parrington et al., 2009] have opted to perform the suboptimal Kalman filtering step (12) in the logarithm of the concentrations:

$$\log \mathbf{x}^a = \log \mathbf{x}^f + \mathbf{K}\left(\widehat{\mathbf{z}} - \mathcal{H}\left(\mathbf{x}^f\right)\right)$$

Here $\mathbf{K}$ is the Kalman gain matrix, $\mathcal{H}$ is the observation operator defined in equation (16), and $\hat{\mathbf{z}}$ is the ozone profile retrievals from TES as described in equation (15). The

analysis state is calculated in natural logarithm of volume mixing ratio (log VMR) at each observation location since the TES profile retrievals are in log VMR. An exponential operator and a linear interpolation operator based on pressure is then applied to this logarithm of analysis state in succession, to regain the actual analysis state in GEOS-Chem grid domain. The model grid points which do not lie on the observation locations in observation space remain unaffected by the assimilation.

The observation operator $\mathcal{H}$ that transforms higher resolution model state to the TES profile vertical grid (observation grid) domain is expressed by equation (16). The Kalman gain matrix $\mathbf{K}$ is defined by equation (13), particularized to the case where the state is the logarithm of volume mixing ratio.

For variational data assimilation the forcing calculation is carried out in concentrations. For this reason, an adjoint of the observation operator needs to be derived to update the gradients as described in equations (7) and (11)

$$\mathbf{H}^T \cdot \mathbf{v} = \left(\frac{\partial}{\partial \mathbf{x}} \left(\mathbf{A} \log \left(\mathbf{L}\,\mathbf{x} \right) \right) \right)^T \cdot \mathbf{v} = \mathbf{L}^T \cdot \begin{pmatrix} (\mathbf{L}\mathbf{x})_0^{-1} & 0 & \cdots & 0 \\ 0 & (\mathbf{L}\mathbf{x})_1^{-1} & \cdots & 0 \\ \vdots & \vdots & \ddots & \vdots \\ 0 & 0 & \cdots & (\mathbf{L}\mathbf{x})_P^{-1} \end{pmatrix} \cdot \mathbf{A}^T \cdot \mathbf{v}$$

Here, $\mathbf{H} = \mathcal{H}'(\mathbf{x})$ is a matrix and $\mathbf{v} = \mathbf{R}^{-1}\ (\mathcal{H}(\mathbf{x}) - \mathbf{y})$. The TES averaging kernel $\mathbf{A}$ is usually a non-symmetric matrix, and the result of $\mathbf{A}^T \cdot \mathbf{v}$ is fed to the interpolation operator to construct the diagonal matrix with the i-th element being $1/(\mathbf{L}\mathbf{x})_i$. The term $\mathbf{L}^T$ is the adjoint of the interpolation operator and brings entities from the TES profile retrieval domain back to the GEOS-Chem model domain.

Note that the TES data can be biased by as much as 10% [Nassar et al., 2008]. We have estimated the bias using the technique proposed in Nassar et al. [2008] and have removed it before assimilating the data.

5. Experimental setting for data assimilation

For numerical experiments, we employ GEOS-Chem v7-04-10 adjoint code package [Singh et al., 2009b], capable of performing both 3D-Var and 4D-Var data assimilations with real data. It also incorporates suboptimal Kalman filter approach of data assimilation developed in Parrington et al. [2009]. We assimilate Tropospheric Emission Spectrometer (TES) satellite ozone profile retrievals into the GEOS-Chem model and validate the generated analyses against an independent observation dataset provided by direct ozone profile measurements from ozonesondes. The numerical optimization method used in all variational experiments is the limited memory bound-constrained BFGS [Zhu et al., 1997]. This quasi-Newton approach has become the "gold standard" in solving large scale chemical data assimilation problems [Sandu et al., 2005a].

The 3D-Var and suboptimal KF frameworks use Sparse Matrix Vectorized GEAR (SMVGEAR) solver for chemistry. However, to construct the adjoint of chemistry required by the 4D-Var, we implemented the Kinetic PreProcessor (KPP) solver [Damian et al., 2002] into GEOS-Chem which not only provides a suite of high performance chemical solvers to choose from but also generates automatically the continuous and discrete adjoint codes [Daescu, 2000, 2003; Sandu et al., 2003a, b]. A detailed discussion on interfacing KPP with GEOS-Chem and comparison with native SMVGEAR solver for accuracy and computational performance is presented in Eller et al. [2009]. Thus, 4D-Var has KPP, and 3D-Var and suboptimal KF have SMVGEAR as their underlying chemistry solvers.

The GEOS-Chem model over which the three assimilation methods are built upon, has been modified further to use the linearized ozone (linoz) scheme [McLinden et al.,

2000] for a better estimate of ozone exchanges at troposphere-stratosphere boundary. This scheme is available in GEOS-Chem v8 and higher (see `http://geos-chem.org`).

Simulations with GEOS-Chem v7-04-10 adjoint can be carried out at $4^\circ \times 5^\circ$ and $2^\circ \times 2.5^\circ$ resolutions. We have used $4^\circ \times 5^\circ$ resolution in all our experiments. There are 46 x 72 latitude-longitude grid boxes at this resolution, and 55 vertical levels. Near the equator and at ground level each grid box covers an area of about 400 km $\times$ 500 km. We performed data assimilation for only the first 23 model levels (for up to about 50 hPa), which encompasses where TES observations are most sensitive.

5.1. Assimilation window lengths

The TES data in all our data assimilation experiments were read once every four simulation hours; the observation operator called at model time t (hours) reads in all the measurements collected within the interval $t-2$ (hours) to $t+2$ (hours). This collective reading increases computational efficiency since reading through observation data files is an expensive process. However, this assumes that the model state does not vary significantly in a four hour time interval which is true in our case as we are using global GEOS-Chem model with $4^\circ \times 5^\circ$ resolution.

3D-Var data assimilation experiments were performed for a period of two weeks in the month of August 2006, starting at 00:00(GMT) on August 1st. The assimilation treats all observations in the four hour interval as instantaneous, and assimilates them in the same optimization run. In all our 3D-Var experiments, we performed 8 iterations per analysis since the cost function decreased significantly within the first few iterations. It is important to note that 3D-Var does not involve any model ad-

joint calculations; gradients require only the adjoint of the observation operator. The optimization adjusts the ozone concentrations. Generated analysis profile at the end of each observation window is evolved through the forward model that becomes the initial condition for the next observation window. It is also worth mentioning that these new initial conditions are used to construct a new background error covariance matrix (17) every observation window.

The setup for data assimilation using the suboptimal Kalman filter is quite similar to 3D-Var where we assimilated TES profile retrievals into GEOS-Chem over a two week period from 00:00 GMT on August 1, 2006 to 00:00 GMT on August 15, 2006. Observations were read every 4 hours and analysis states were generated for each observation window through the sequential update formula (12).

The 4D-Var data assimilation experiments were performed for two different assimilation window lengths to adjudge if model errors hamper the quality of assimilations in GEOS-Chem involving longer assimilation windows; 4D-Var is strongly constrained by the forward model equation (10). Starting at 00:00 GMT on August 1, 2006, the first assimilation window is considered to be of five days while the second window is of two weeks. All the three assimilation systems had the same initial conditions to start with and were generated through a free GEOS-Chem model run. There were 12 optimization iterations performed in order to improve the ozone initial condition. Each iteration during 4D-Var assimilation includes a forward model and a backward model adjoint run. TES profile retrievals were read every 4 hours during the model adjoint run, and the cost function and adjoint gradients accumulated the impact of all 4 hour data sets throughout the assimilation window. Unlike 3D-Var

and suboptimal KF, where analysis states are generated sequentially every observation window, 4D-Var produces new initial conditions that could be used by the model to generate analysis at any time during the assimilation window.

To assess the quality of analysis generated by the above mentioned assimilation techniques, we provide in section 6.2, various plots including comparison of analyses against ozonesonde observations and global ozone distribution for 5 days and 2 weeks assimilation windows. It is important to note that, since 3D-Var and suboptimal KF are sequential in nature, we did not have to run 5 days assimilation for these two methods separately. Rather, we used the saved analyses generated during the 2 weeks assimilation.

5.2. Specification of background error variances

We consider a diagonal background error covariance matrix (**B**) in all our variational data assimilation experiments for simplicity. The initial variances (the diagonal entries of the **B** matrix) are constructed from the average background concentrations $\mathbf{x}_0^B$ on each of the Nlev model vertical layers

$$\mathbf{B} = \begin{bmatrix} \mathbf{B}^{(0)} & 0 \dots & 0 \\ 0 & \mathbf{B}^{(1)} \dots & 0 \\ \vdots & \ddots & \vdots \\ 0 & 0 \dots & \mathbf{B}^{(\mathrm{Nlev})} \end{bmatrix} \tag{17}$$

where

$$\mathbf{B}^{(\ell)} = \begin{bmatrix} \sigma_\ell^2 & 0 \dots & 0 \\ 0 & \sigma_\ell^2 \dots & 0 \\ \vdots & \ddots & \vdots \\ 0 & 0 \dots & \sigma_\ell^2 \end{bmatrix}_{\dim \times \dim}, \quad \dim = \mathrm{Nlon} \cdot \mathrm{Nlat}, \tag{18}$$

with

$$\sigma_\ell = \frac{\alpha_{\mathrm{rel}}}{\dim} \sum_{i=1}^{\mathrm{Nlon}} \sum_{j=1}^{\mathrm{Nlat}} \mathbf{x}_0^B(i,j,\ell,s_{O3}), \quad \ell = 1, \cdots, \mathrm{Nlev}, \quad s_{O3} = \text{index of ozone}. \tag{19}$$

The relative uncertainty level in the background initial conditions (i.e., at the beginning of the assimilation window) is taken to be 50%, i.e., $\alpha_{\text{rel}} = 0.5$.

The forecast error covariance matrix $\mathbf{P}^f$ used in our suboptimal Kalman filter approach is diagonal. The initial forecast error is assumed to be 50% of the initial forecast field that is supposed to capture the representativeness error as well. In matrix form, $\mathbf{P}_0^f$ is represented as

$$\mathbf{P}_0^f = \begin{bmatrix} \mathbf{P}_0^{f^{(0)}} & 0 \dots & 0 \\ 0 & \mathbf{P}_0^{f^{(1)}} \dots & 0 \\ \vdots & \ddots & \vdots \\ 0 & 0 \dots & \mathbf{P}_0^{f^{(\text{Nobs})}} \end{bmatrix} \tag{20}$$

where Nobs is the number of observation locations (in our case, the number of grid points in the TES retrieval domain). The initial forecast error covariance matrix block corresponding to each observation location is given as

$$\mathbf{P}_0^{f^{(i)}} = \alpha_{\text{rel}}^2 \cdot \begin{bmatrix} (\mathbf{x}_0^f(i,1,s_{O3}))^2 & 0 & \dots & 0 \\ 0 & (\mathbf{x}_0^f(i,2,s_{O3}))^2 & \dots & 0 \\ \vdots & \ddots & & \vdots \\ 0 & 0 & \dots & (\mathbf{x}_0^f(i,\text{Nret},s_{O3}))^2 \end{bmatrix}_{\text{Nret}\times\text{Nret}}, \tag{21}$$

for $i = 1, 2, \dots, \text{Nobs}$, and where Nret is the number of vertical TES profile retrieval levels. Although the initial forecast error covariance matrix $\mathbf{P}^f$ and all analysis $\mathbf{P}^a$s henceforth are diagonal and there are no spatial correlations being accounted for; the averaging kernels in the observation operator of TES as defined in equation (16) provide vertical correlations when operated on $\mathbf{P}^f$ through equation (13). A detailed discussion on how to efficiently extend the background error covariance matrices to non-diagonal forms that capture spatial error correlations is provided in Singh et al. [2010a].

6. Data assimilation results

6.1. Computational costs

As pointed out in Henze et al. [2007], the computational cost of Rosenbrock solver increases significantly with the tolerance levels; higher tolerances use smaller internal time steps requiring more computation. Therefore, in our experiments, we have set the KPP parameters RTOL=10^{-3} and ATOL=10^{-2} to achieve moderate to high accuracy.

The suboptimal Kalman filter is less expensive than 3D-Var as it generates the analysis through single update formula (12), whereas 3D-Var requires a few iterations before the optimization routine could generate a stable optimal analysis field. This is true however as long as the forecast error covariance matrix is diagonal. Once we move to non-diagonal matrices, the cost of calculating Kalman gain matrix (13) can be high, although this can be parameterized following, for example, Khattatov et al. [2000]. In the case of 3D-Var and 4D-Var, using even full **B** matrix adds a minimal cost to the overall simulation since the complete matrix is never constructed; at each step only a matrix vector product is required and efficient techniques are employed to derive the inverse and other powers of **B** matrix [Singh et al., 2010a]. The 4D-Var assimilation is the most expensive of all the assimilation systems under consideration. The reason is attributed to the fact that a single 4D-Var iteration performs both the forward and adjoint model runs, where, several variables on which the adjoint equation depends on, are written in checkpoint files during forward model run and read during adjoint model run. In our study, a full adjoint run for one simulation day requires about 12 GB of hard drive storage. This consumption could be reduced by almost 50% if rather than saving intermediate concentrations of chemical integration,

they are recalculated by calling forward chemistry in the adjoint run, which would eventually lead to higher computational time.

Table 1 provides a comparison of the computational costs of the different data assimilation systems and the cost of free running model for a 24 hour simulation. All the simulations are performed on a Dell Precision T5400 workstation with two quad-core Intel(R) Xeon(R) processors, with clock speed 2.33GHz, and 16GB of RAM shared between the two processors.

6.2. Comparison with ozonesonde measurements

In order to assess the quality of analysis fields generated through different assimilation systems, we use ozonesonde profiles measured by the INTEX Ozonesonde Network Study 2006 (IONS-6) (`http://croc.gsfc.nasa.gov/intexb/ions06.html`, [Thompson et al., 2007a, 2007b]) for the month of August, assuming that these measurements provide values close to the true state of the atmosphere. There are 418 ozonesondes launched from 22 stations across North America as shown in the Figure 1. A detailed description of the number of ozonesondes launched per station with longitude and latitude information can be found in Parrington et al. [2008]. The ozonesonde observations are not used in data assimilation, and therefore provide an independent data set against which the analysis results are validated. Forecast scoring techniques as described in Wu et al. [2008]; Constantinescu et al. [2007c] that use assimilated data for validation, do not provide a fair assessment of the quality of assimilation for sparse spatio-temporal sampling and longer time scales used in this analysis.

We first consider the case where the assimilation window length is five days. As per the property of sequential data assimilation algorithms, the model forecast is corrected as soon as an observation is available. Ingesting observations every four simulation hours, we obtain an analysis field every four hours that accounts for the mismatch between the model prediction and the observations within that observation window. However, it is important to note that the model prediction at any observation window incorporates implicitly the corrections from all previous observations. Thus, as we move forward in time, the analysis field agrees better with the true state of the atmosphere. 4D-Var on the other hand accumulates the forcing due to mismatch between model forecast and observations throughout the assimilation window to produce an initial condition that, when evolved forward in time through the model, will best fit the observations. Therefore, in the case of sequential assimilation approaches, to obtain a stable analysis state that resembles the true chemical state of the atmosphere at a particular instant, we need to start the simulation days or months prior to that instant to benefit from earlier observations. 4D-Var is advantageous in situations where past observations are not available, as it provides the best estimate using only the observations available in the assimilation window under consideration.

We present in Figure 2, a comparison of analysis profiles obtained from different assimilation systems, and free GEOS-Chem model run against ozonesonde measurement data. The left panel shows vertical ozone profiles (concentrations against pressure levels); the model predictions are sampled at the locations and times of ozonesonde measurements available in the 5-day assimilation window. The differences between model results and ozonesonde data reflect model prediction errors;

one error vertical profile is obtained for each ozonesonde launch. The center and right panels show the mean and the standard deviation of these errors. The plots provide an assessment of the quality of tropospheric ozone estimates given by the free model run, and by data assimilation systems based on suboptimal Kalman filter, 3D-Var and 4D-Var approaches. The errors also reflect the impact of TES profile retrievals on these assimilation systems.

It is evident from the plots in Figure 2 that 4D-Var provided the best estimate for lower and mid troposphere ozone concentrations. The relative difference between the mean ozone analysis field and the ozonesonde measurements were decreased to less than 4% up to 180 hPa as compared to 5-20% in cases of suboptimal KF and 3D-Var. The overestimate of ozone in the upper troposphere is likely due to the accumulated impact of the TES bias. The bias correction approach described in Nassar et al. [2008] may not be sufficient for assimilation studies and suggests an on-line bias correction scheme may be needed in the future.There was also a substantial improvement in the variance of the assimilation relative to the ozonesonde measurements, particularly for the 4D-Var case at 200 hPa. Consequently, the satellite observations have an impact not only on the mean value of tropospheric ozone but they also provide additional information on the ozone variability. A detailed analysis on the information brought in by TES profile retrievals into 4D-Var assimilation system at different pressure levels is provided in Singh et al. [2010b].

Figure 3 provides the global tropospheric ozone distribution as estimated by GEOS-Chem free model run and different assimilation systems at the end of the 5 days assimilation window. The ozone concentration values are averaged over 10 GEOS-

Chem levels (from the surface to about 370 hPa) for each longitude-latitude grid point on the horizontal domain.

As seen in Figure 3, all the assimilation systems seem to have caused an increase in the tropospheric ozone as compared to the model forecast with 4D-Var bringing the highest amount. The gain seems to be prominent in the 30° N to 60° N latitude region in case of suboptimal KF and 3D-Var, while it is extended up to 90° N in case of 4D-Var. For a clear demonstration of these changes, we provide in Figure 4, the plots of differences in the tropospheric ozone estimates through free model run and different assimilation systems.

In Figure 4, panels (a) and (b) show that the structure of corrections in the ozone concentrations through 3D-Var and suboptimal KF data assimilation are quite similar. The reason behind such a structure is that these sequential algorithms bring in instantaneous corrections based solely on the mismatch between the model predictions and the observations in an observation window (analysis cycle). The localized corrections here are mostly along the Aura satellite orbit. Panel (c) on the other hand showcases the smoother correction profile of 4D-Var. In each 4D-Var optimization iteration, the cost function and gradients are accumulated for all the observation windows where the adjoint variable (gradient) is flown backwards in time as governed by the model adjoint equation. The corrections brought in by the optimization routine therefore are no longer localized resulting in an ozone distribution consistent with the model dynamics and chemistry. We also plot the difference in the analysis fields obtained by 3D-Var and suboptimal KF showcasing their close resemblance (panel (d)). Interestingly, there seems to be a localized overcorrection in the mid west Australian region

by the suboptimal Kalman filter. This overcorrection is likely due to the propagation of emissivity errors over Australian desert in the TES retrieval, which can have possess strong silicate spectral signatures into the TES ozone retrieval. While in case of 4D-Var, the underlying algorithm can smooth out localized satellite artifacts through strong model constraints.

We next consider assimilation window length of 2 weeks. A longer assimilation window provides an insight into how ozone estimates provided through assimilation evolve with time and if the corrections maintain structures similar to 5-day case. In particular, the ozone lifetime will limit the utility of ozone initial condition adjustment as the assimilation window increases. It also helps adjudge if model errors in GEOS-Chem cause any degradation in the assimilation systems, especially the strongly constrained 4D-Var. Similar to Figure 2, we present in Figure 5, a comparison of analysis profiles obtained from different assimilation systems against ozonesonde measurement data. The plots reflect that the accuracy of suboptimal Kalman filter and 3D-Var assimilations start to differ with longer assimilation window. While suboptimal KF underestimates ozone concentrations in the lower and mid troposphere, it performs better than 3D-Var in the mid and upper tropospheric region. 4D-Var still provides the best ozone estimate of all the assimilation systems, and, unlike the 5 days assimilation window length case, it performs well in the upper tropospheric region except near the tropopause. Panel (c) suggests that the standard deviation of 4D-Var analysis from the ozonesonde measurements stayed the least among all the assimilation systems. The relative difference between the mean ozone analysis field and the ozonesonde measurements were decreased to less than 4% up to 150 hPa as

compared to 4-16% in cases of suboptimal KF and 3D-Var. With longer assimilation window, all the assimilation systems seem to have benefited from more observations being assimilated.

Figure 6 provides the global tropospheric ozone distribution as estimated by GEOS-Chem free model run and different assimilation systems. Similar to the 5 days assimilation window case, 4D-Var leads to the maximum increase in the tropospheric ozone.

Figure 7 showcases the structure of corrections in model predicted ozone through different assimilation systems. The ozone corrections are up to 20 ppbv, and are consistent among the three assimilation schemes. The localized correction structure in 3D-Var and suboptimal KF cases still persists with longer assimilation window. 4D-Var provides larger corrections with a significant increase in ozone concentrations in the 30° N to 90° N latitude region. The reason for this difference can be explained in part by the restriction of the TES to 60°S-60°N, which limits where the corrections can be made in the 3D-Var. Changes poleward of 60°N in the 3D-Var solution are due to forward advection. However, as discussed in Section 6.3.2, the elevated ozone poleward of 60°N in the 4D-Var solution is due to the positive correction of high latitude initial conditions at the beginning of the assimilation window at August 1, 2006.

The overcorrection in the mid west Australian region which was not visible in the 3D-Var case for 5 days assimilation window, seems to be prominent in longer assimilation, while, for suboptimal KF, it has been accentuated. The fact that this phenomenon is seen only in 3D-Var and suboptimal KF could be attributed to the propagation of

emissivity errors described earlier, combined with the localized correction property of these methods. Differences in the amount of overcorrection in the two methods could be attributed to differences in their implementations. For example, as described in section 2.3, the forecast error variances at observation time $i+1$ in the suboptimal KF case, are constructed by transporting variances at observation time i as passive tracers, while in case of 3D-Var, they are generated from the current model state. Also, the KF implementation used in this study solves the underlying statistical problem generating analysis in observation space, then maps the solution back to the model space. While in 3D-Var, the same statistical problem is solved in the model space itself, leading to different forecast error covariance matrices.

Contrary to what was observed in Wu et al. [2008] for the 4D-Var assimilation in Polair3D case (where accuracy of the ozone estimates decreased with increase in the assimilation window length), our findings show that the performance of 4D-Var system improves with increase of the assimilation window length. However, this is likely due to the fact that ozone lifetime is reasonably close to two weeks. Assimilation windows longer than two weeks would lead to a reduction in performance of the 4D-Var system as the initial conditions become less important towards the end of the window. Consequently, the assimilation window for ozone in a 4D-Var system should be bounded by the ozone lifetime. There is however one case where the accuracy of ozone estimates decrease with increase in assimilation window length for 4D-Var and that is when the model adjoints are inaccurate. We have studied this case in detail in Singh et al. [2010c] and have utilized inaccurate gradients to work toward our

benefit in terms of reducing significantly the memory and computational costs, still maintaining the quality of the analysis.

6.3. Comparison of 3D-Var and 4D-Var

As discussed in Section 2, the 3D-Var approach processes observations sequentially, and generates a new analysis every time new observations are available. The 3D-Var corrections perform successive adjustments of the forward model trajectory, which decrease the error as more observations are being considered. The 4D-Var approach, on the other hand, processes all observations at once and adjusts the initial conditions for the current assimilation window. It is also worth reiterating that the background error covariance matrix in 4D-Var is static and flow independent, while in case of 3D-Var, it is constructed every observation time through model evolution of the analysis generated at previous observation time.

We compare the 3D-Var and 4D-Var approaches in two different ways. Section 6.3.1 discusses the ability of 4D-Var to explicitly represent relationships between different chemical components. Section 6.3.2 proposes a variational approach to directly compare the use of information by the two methods.

6.3.1. Dependencies between multiple species

The data assimilation scenario discussed here corrects ozone distribution in response to new information provided by ozone measurements. This correction is distributed implicitly to other state variables (e.g., other dependent chemical species) through model evolution.

In order to perform explicit corrections to other chemical species, 3D-Var requires an inter-species error correlation matrix. A correct specification of such matrix at each

observation time is a difficult task. 4D-Var approach on other hand captures the relationship between species through model adjoint dynamics. This holds true even when the background error covariance matrix does not specify inter-species correlations. It is possible to directly extend the set of control variables to include initial conditions of all chemical species present in the model, together with the emission and deposition rates, and any other model parameters. There is no additional computational cost since the adjoint model already computes derivatives with respect to all the state variables. (Of course, extending the control vector may lead to separate issues related to convergence, and to proper regularization of the problem).

The adjoint sensitivity analysis by itself is an important tool to investigate various dependencies between model parameters. The gradient formula (11) provides derivatives of the cost function with respect to initial conditions of other species besides ozone, and with respect to model parameters such as emissions and boundary conditions. The derivatives with respect to model parameters are obtained by post-processing the adjoint variables [Sandu et al., 2005a]. The units of adjoint sensitivities with respect to a parameter are one over the unit of that parameter since the cost function (9) is unitless. Scaled adjoint sensitivities (e.g., $\nabla_{\mathbf{x}_0}\mathcal{J} \odot \mathbf{x}_0^{\mathrm{a}}$, where $\odot$ is component-wise multiplication) are unitless, and measure the impact of *relative* changes in parameters on the cost function.

Figure 8 presents the scaled adjoint sensitivities of the 4D-Var cost function (9) with respect to several model parameters. The linearization is performed around the 4D-Var solution (10), i.e., around a forward trajectory that starts with optimized initial ozone concentrations. Consequently, the sensitivity of the 4D-Var cost function with

respect to the initial ozone concentration is very small (in theory is equal to zero, as it represents the gradient value at a minimum point). The sensitivities with respect to initial CO, NO_X, and PAN concentrations are presented in Figures 8 (a),(b), and (c) respectively. These sensitivities are far from zero; consequently, TES ozone profiles provide information that can potentially constrain ozone precursor initial conditions as well. (This can be achieved by extending the vector of control variables to include the initial conditions of additional species, and continuing the optimization. Large scaled gradient components corresponding to initial CO, NO_X, and PAN indicate that changes in these initial conditions lead to a considerable decrease in model-observation mismatch). Additional information can be obtained from influence functions, which are ratios of scaled sensitivities Fisher and Lary [1995]. More importantly, Figure 8(d) displays the sensitivity of the 4D-Var cost function with respect to total NO_x emissions. These sensitivities indicate that ozone observations can be used to constrain ozone precursor emissions as well. This point is explored in the context of a 4D-Var chemical box model in Hamer et al. [2011]. The strong sensitivity of the atmospheric chemical state to boundary conditions differentiates the chemical data assimilation problem from the traditional numerical weather prediction problem. Consequently, even in condition where the 3D-Var solution may have similar performance to the 4D-Var solution, the ability to assess the sensitivities of the innovations in the 3D-Var to boundary and initial conditions through adjoint calculations provides important tools for a more detailed investigation of processes controlling that distribution.

6.3.2. Direct comparison of 3D-Var and 4D-Var corrections

Due to the different times when they incorporate observations, it is difficult to perform a direct comparison of the ways 3D-Var and 4D-Var use this information. An assessment of the two analyses can be done at the end of the assimilation interval. Comparison against ozonesonde data, presented in Figures 2 and 5, use analysis data at different times throughout the assimilation window.

We propose a variational approach to compare the net effect of all corrections performed by the 3D-Var, with the 4D-Var correction of the state. This comparison provides insight into how each method injects information from observations into the state (at a specific time). We discuss three approaches, based on "pulling back" to the initial time and adding all corrections performed by 3D-Var, pulling back and adding all the differences between the 3D-Var and the 4D-Var analyses, and finding an equivalent initial condition for 3D-Var.

To be specific, we first quantify the cumulative effect of all 3D-Var corrections, in order to study how 3D-Var builds the analysis. Since the 3D-Var corrections take place at different times, they need to first be brought to the same time. For example, this can be done done by "propagating backwards" the 3D-Var correction at t_i to the initial time t_0, through the adjoint $\mathbf{M}_i^T$ of the tangent linear model $\mathbf{M}_i = \partial \mathbf{x}_i / \partial \mathbf{x}_0$. The cumulative effect of all 3D-Var corrections at the initial time is

$$\sum_{i=0}^{N} \mathbf{M}_k^T \cdot \mathbf{P}_i^{f(3)} \mathbf{H}_i^{\mathrm{T}} \left(\mathbf{H}_i \mathbf{P}_i^{f(3)} \mathbf{H}_i^{\mathrm{T}} + \mathbf{R}_i \right)^{-1} \left(\mathbf{y}_i - \mathcal{H}(\mathbf{x}_i^{f(3)}) \right) . \tag{22}$$

Here $\mathbf{x}_i^{f(3)}$ and $\mathbf{P}_i^{f(3)}$ are the 3D-Var forecast state and the forecast covariance at t_i, respectively. This approach allows for the assessment of the cumulative effect of all 3D-Var corrections at the initial time, and to directly compare the 3D-Var and 4D-Var via the corresponding changes in initial conditions.

Next, we seek to estimate the discrepancy between the analyses generated by the 3D-Var and by the 4D-Var methods. Let the free model run (background), the 4D-Var, and the 3D-Var analyses at t_i be $\mathbf{x}_i^b$, $\mathbf{x}_i^{a(4)}$, $\mathbf{x}_i^{a(3)}$, respectively. Define the following "discrepancy" cost function that measures the difference between the 4D-Var and the 3D-Var analyses at all times

$$\mathcal{D}\left(\mathbf{x}_0^{a(4)}\right) = \frac{1}{2}\sum_{i=0}^{N}\left\|\mathbf{x}_i^{a(4)} - \mathbf{x}_i^{a(3)}\right\|^2_{\mathbf{Q}_i^{-1}} . \tag{23}$$

The gradient of the discrepancy function with respect to the initial conditions is given by the adjoint model, using a linearization of the forward model about the 4D-Var analysis trajectory

$$\nabla_{\mathbf{x}_0^a}\mathcal{D}\left(\mathbf{x}_0^{a(4)}\right) = \sum_{i=0}^{N}\mathbf{M}_i^T\,\mathbf{Q}_i^{-1}\,\left(\mathbf{x}_i^{a(4)} - \mathbf{x}_i^{a(3)}\right), \quad \text{where} \mathbf{M}_i = \frac{\partial \mathbf{x}_i^{a(4)}}{\partial \mathbf{x}_0^{a(4)}} . \tag{24}$$

Here $\mathbf{M}_i$ is the linearized model solution operator about the 4D-Var analysis trajectory. Each term in the discrepancy sum is weighed by the (covariance-like) matrix $\mathbf{Q}_i$, which is assumed to be invertible. This adjoint considers the differences between the 4D-Var and the 3D-Var analyses at different times, and pulls all these differences back to time t_0. The cumulative discrepancy between the two analyses, as given by this metric, reads

$$\text{diff}\left(\mathbf{x}^{a(4)}, \mathbf{x}^{a(3)}\right) = \nabla_{\mathbf{x}_0^a}\mathcal{D}\left(\mathbf{x}_0^{a(4)}\right) . \tag{25}$$

Finally, we want to determine the "3D-Var equivalent initial condition" $\mathbf{x}_0^{e(3)}$, such that the resulting trajectory $\mathbf{x}_i^{e(3)}$, $i \geq 1$, fits best the 3D-Var analysis at the final time $\mathbf{x}_N^{a(3)}$, in a least squares sense:

$$\mathbf{x}_0^{e(3)} = \arg\min_{\mathbf{x}_0}\ \mathcal{B}\left(\mathbf{x}_0^{e(3)}\right) = \frac{1}{2}\left\|\mathbf{x}_N^{a(4)} - \mathbf{x}_N^{a(3)}\right\|^2_{\mathbf{Q}_N^{-1}} .$$

To our knowledge, no attempt has been made to date to estimate the equivalent effect of all 3D-Var corrections at the initial time. (Note that the 3D-Var analysis is not a trajectory of the model). The methodology is explained in Appendix A. The least squares solution to finding the 3D-Var equivalent initial condition is (A3)

$$\mathbf{x}_0^{e(3)} = \mathbf{x}_0^{a(4)} - \left(\mathbf{M}_N^T \mathbf{Q}_N^{-1} \mathbf{M}_N\right)^{-1} \cdot \mathbf{M}_N^T \mathbf{Q}_N^{-1} \left(\mathbf{x}_0^{a(4)} - \mathbf{x}_0^{a(3)}\right) ,$$

The 3D-Var solution incorporates all the observation information when it reaches t_N, the end of the assimilation window. For a direct comparison with the 4D-Var initial condition, the 3D-Var equivalent initial condition match the 3D-Var analysis only at the final time.

Similar to (23), a cost function that measures the discrepancy between the 3D-Var and the free model forecast at all times can be defined. This gradient involves an adjoint run, with a linearization performed about the free model run (background) trajectory.

Figure 9 displays results for the metric (25), i.e., the sum of all analysis discrepancies between the 3D-Var and the 4D-Var ozone analyses, projected to time t_0 along with differences between the free running model and the initial conditions inferred from the 4D-Variational solution. All scaling covariances are taken to be identity matrix, $\mathbf{Q}_i = \mathbf{I}$, $i = 0, \ldots, N$. It is interesting to note that, significant corrections to the initial conditions in the 4D-Var solution are made poleward of 60°N even though there is no TES data used that directly covers that region. These positive corrections can be explained by strong transport from higher latitudes into the mid-latitudes characterized by the transport adjoint sensitivities of the mid-latitude innovations with the TES

data. Similar features are seen though in the opposite sign in Figure 9(d) through the cumulative back projection in the 3D-Var solution.

7. Conclusions

This paper compares the performance of 3D-Var, 4D-Var, and suboptimal Kalman filter data assimilation systems, applied to the estimation of global tropospheric ozone distribution. The data is provided by TES ozone profile retrievals. The study uses the 3D-Var and 4D-Var data assimilation frameworks we have implemented into GEOS-Chem v7. Two different assimilation window lengths (five days and two weeks) are considered. The quality of the ozone analyses provided by different assimilation schemes is verified against ozonesonde measurements, an independent data set.

The three approaches have different computational costs. The suboptimal Kalman filter is the least expensive, followed closely by 3D-Var. 4D-Var has the highest memory and computational costs as it requires checkpointing dependent variables, and performs both a forward and an adjoint model run for every iteration.

All three data assimilation systems are able to improve ozone estimates using TES profile retrievals. For the five days assimilation window the sequential methods, 3D-Var and suboptimal KF, perform similarly: they decrease the relative difference between mean analysis and ozonesonde measurements to about 5-20%. 4D-Var, on the other hand, brings this error down to less than 4%, for up to 180 hPa. For the two weeks assimilation window the performance of the sequential methods changes with different height levels. In the lower and mid troposphere 3D-Var performs better, while in the mid to upper troposphere the suboptimal Kalman filter analysis is more accurate. The relative error (measured against ozonesonde data) is 4-16% for the se-

quential analyses, and is less than 4% for up to 150 hPa for 4D-Var. The corrections of ozone concentration performed by the sequential assimilation methods are localized along the satellite orbit. On the other hand, the 4D-Var solution is physically and chemically self-consistent over the assimilation window. The region between latitudes 30° N to 60° N has the greatest impact from all the assimilation systems. This region extends up to 90° N in case of 4D-Var, which accounts for the transport of high latitude ozone into the mid-latitudes. However, we should caution that the IONS datasets were primarily over North America. Therefore, we can not assess whether the increased northern mid-latitude ozone concentrations lead to a more accurate analysis.

A method to directly compare the analyses provided different schemes is proposed, based on "pulling back" differences to the initial time, as discussed in Section 6.3.2. The calculations show that the 4D-Var corrections are larger than those provided by 3D-Var. The adjoint sensitivity analysis in section 6.3.1 reveals that 4D-Var has the intrinsic capability of capturing mechanistic relationships between multiple chemical species, and between emissions and concentrations fields. In a similar vein, this adjoint analysis can be used in conjunction with other assimilation schemes (3D-Var, suboptimal KF) to interrogate what model parameters are driving the residual differences with the observations.

The comparison results presented here will guide the choice of the best assimilation scheme for the problem at hand. The sub-optimal Kalman filter and the 3D-Var solution provide useful solutions that do not require significant changes as the forward model physics and chemistry are updated. By virtue of their simplicity, they

make less model assumptions, e.g., all differences between observation and forecast can be attributed to initial conditions, and therefore can be robust under a variety of conditions. On the other hand, the 4D-Var approach provides a physically consistent solution where uncertainties are ascribed to a combination of initial and boundary conditions. This physical consistency makes it more straightforward to interpret and make scientific inferences. We have introduced a new method that applies the adjoint sensitivity to help interpret the 3D-Var solutions, which provides a kind of middle ground between the more efficient 3D-Var approach and the more sophisticated 4D-Var approaches. Interesting extensions of the GEOS-Chem data assimilation framework, such as efficient information content estimation of observations and construction of full rank covariance matrices, are discussed in companion papers Singh et al. [2010a, b, c].

Acknowledgments. This work was supported by NASA through the ROSES-2005 AIST project. The work of A. Sandu was also partially supported by NSF through the award NSF DMS–0915047. The authors would like to thank Professor Anne Thompson of Pennsylvania State University and Dr. David Tarasick of Environment Canada who led the IONS-6 campaign, and who provided the IONS data used in this work.

References

Beer, R., Glavich, T. A., and Rider, D. M.: Tropospheric emission spectrometer for the Earth Observing System's Aura satellite, Appl. Opt., 40(15), 2356-2367, 2001.

Bei, N., de Foy, B., Lei, W., Zavala, M., and Molina, L. T.: Using 3DVAR data assimilation system to improve ozone simulations in the Mexico City basin, Atmos. Chem.

Phys., 8, 7353-7366, doi:10.5194/acp-8-7353-2008, 2008.

Benkovitz, C. M., Scholtz, M. T., Pacyna, J., Tarrason, L., Dignon, J., Voldner, E. C., Spiro, P. A., Logan, J. A., and Graedel, T. E.: Global gridded inventories of anthropogenic emissions of sulfur and nitrogen, J. Geophys. Res., 101(D22), 29,239-29,253, 1996.

Bey, I., Jacob, D. J. , Yantosca, R. M., Logan, J. A., Field, B., Fiore, A. M., Li, Q., Liu, H., Mickley, L. J. and Schultz, M.: Global modeling of tropospheric chemistry with assimilated meteorology: Model description and evaluation, J. Geophys. Res., 106, 23, 073-23,096, 2001.

Blum, J., Le Dimet, FX., Navon, I. M.: Data Assimilation for Geophysical Fluids, Chapter in Computational Methods for the Atmosphere and the Oceans, Volume 14, Elsevier Science Ltd, New York, ISBN-13: 978-0-444-51893-4, 2009.

Boutahar, J., Lacour, S., Mallet, V., Quélo, D., Roustan, Y., and Sportisse, B.: Development and validation of a fully modular platform for numerical modelling of air pollution: POLAIR, International Journal of Environment and Pollution, 22(1/2):17-28, 2004.

Bowman, K. W., Worden, J., Steck, T., Worden, H. M., Clough, S. and Rodgers, C.: Capturing time and vertical variability of tropospheric ozone: A study using TES nadir retrievals, J. Geophys. Res.,107, (D23), 2007.

Bowman, K. W., Rodgers, C. D., et al: Tropospheric Emission Spectrometer: Retrieval method and error analysis, IEEE Transactions on Geoscience and Remote Sensing, vol. 44, no. 5, May 2006.

K. W. Bowman, D. B. A. Jones, J. A. Logan, H. Worden, F. Boersma, R. Chang, S. Kulawik, G. Osterman, P. Hamer, and J. Worden. The zonal structure of tropical O3 and CO as observed by the Tropospheric Emission Spectrometer in November 2004 Part 2: Impact of surface emissions on O3 and its precursors. Atmos. Chem. Phys., 9(11):3563Ð3582, 06 2009/06/03.

Carmichael, G. R., Sandu, A., Chai, T., Daescu, D., Constantinescu, E. M. and Tang, Y.: Predicting air quality: Improvements through advanced methods to integrate models and measurements, Journal of Computational Physics, Vol. 227, Issue 7, p. 3540–3571, 2008.

Chai, T., Carmichael, G. R., Sandu, A., Tang, Y. and Daescu, D. N.: Chemical data assimilation of transport and chemical evolution over the Pacific (TRACE-P) aircraft measurements, Journal of Geophysical Research, 111, D02301, doi:10.1029/2005JD005883, 2006.

Chai, T., Carmichael, G. R., Tang, Y., Sandu, A., Hardesty, M., Pilewskie, P., Whitlow, S., Browell, E. V., Avery, M. A., Thouret, V., Nedelec, P., Merrill, J. T. and Thomson, A. M.: Four dimensional data assimilation experiments with ICARTT (International Consortium for Atmospheric Transport and Transformation) ozone measurements, Journal of Geophysical Research, Vol. 112, D12S15, doi:10.1029/2006JD007763, 2007.

Chai, T., Carmichael, G. R., Tang, Y. and Sandu, A.: Regional NO_X emission inversion through a four-dimensional variational approach using SCIAMACHY tropospheric NO_2 column observations, Atmospheric Environment, doi:10.1016/j.atmosenv.2009.06.052, in print, 2009.

Clark, H. L., Cathala, M. -L., Teysse'dre, H., Cammas, J. -P. and Peuch.,V. -H.: Cross-tropopause fluxes of ozone using assimilation of MOZAIC observations in a global CTM, Tellus, Ser. A and Ser. B, 59B, 39-49, 2006.

Cohn, S., Da Silva, A., Guo, J., Sienkiewicz, M., and Lamich, D.: Assessing the Effects of Data Selection with DAO's Physical-space Statistical Analysis System, Monthly Weather Review, 126, 2913-2926, 1998.

Constantinescu, E. M., Sandu, A., Chai, T. and Carmichael, G. R.: Investigation of ensemble-based chemical data assimilation in an idealized setting, Atmospheric Environment, Vol. 41, Issue 1, p. 18–36, 2007.

Constantinescu, E. M., Sandu, A., Chai, T. and Carmichael, G. R.: Ensemble-based chemical data assimilation. I: General approach, Quarterly Journal of the Royal Meteorological Society, Volume 133, Issue 626, p. 1229–1243, Online ISSN: 1477-870X, Print ISSN: 0035-9009, July 2007 Part A.

Constantinescu, E. M., Sandu, A., Chai, T. and Carmichael, G. R.: Ensemble-based chemical data assimilation. II: Covariance localization , Quarterly Journal of the Royal Meteorological Society, Volume 133, Issue 626, p. 1245–1256, Online ISSN: 1477-870X, Print ISSN: 0035-9009, July 2007 Part A.

Cooper, O. R., et al.: Large upper tropospheric ozone enhancements above midlatitude North America during summer: In situ evidence from the IONS and MOZAIC ozone measurement network, J. Geophys. Res., 111, D24S05, doi:10.1029/2006JD007306, 2006.

Cooper, O. R., et al.: Evidence for a recurring eastern North American upper tropospheric ozone maximum during summer, J. Geophys. Res., 112, D23304,

doi:10.1029/2007JD008710, 2007.

Courtier, P. and Talagrand, O.: Variational assimilation of meteorological observations with the adjoint vorticity equations II: Numerical results, Quart. J. Roy. Meteor. Soc. 113, 1329-1347, 1987.

Courtier, P., Andersson, E., Heckley, W., Pailleux, J., Vasiljevic, D., Hamrud, M., Hollingsworth, A., Rabier, F. and Fisher, M.: The ECMWF implementation of three-dimensional variational assimilation (3D-Var) I: Formulation, Quarterly Journal of the Royal Meteorological Society, 124(550):1783, 1998.

Daescu, D., Carmichael, G.R., and Sandu, A.: Adjoint Implementation of Rosenbrock Methods Applied to Variational Data Assimilation Problems, J. Comp. Phys, 165, 496-510, 2000.

Daescu, D., Sandu, A., and Carmichael, G.R.: Direct and Adjoint Sensitivity Analysis of Chemical Kinetic Systems with KPP: II - Validation and Numerical Experiments, Atmos. Environ., 37, 5097-5114, 2003.

Daescu, D.N.: On the sensitivity equations of four-dimensional variational (4D-Var) data assimilation, Monthly Weather Review, 136 (8), 3050-3065, 2008.

Daley, R.: Atmospheric Data Analysis, Cambridge University Press, p. 457pp, 1991.

Damian, V., Sandu, A., Damian, M., Potra, F., and Carmichael,G.R.: The Kinetic Pre-Processor KPP - A Software Environment for Solving Chemical Kinetics, Comp. and Chem. Eng., 26, 11, 1567-1579, 2002.

Derber, J. C., Parrish, D. F., Lord, S. J.: The New Global Operational Analysis System at the National Meteorological Center. Weather and Forecasting, 6, 538-547, 1991.

Duncan, B. N., Martin, R. V., Staudt, A. C., Yevich, R., and Logan, J. A.: Interannual and seasonal variability of biomass burning emissions constrained by satellite observations, J. Geophys. Res., 108(D2), 4100, doi:10.1029/2002JD002378, 2003.

Elbern, H., Schmidt, H., and Ebel, A.: Variational data assimilation for tropospheric chemistry modeling, J. Geophys. Res., 21, 15,967-15,985, 1997.

Elbern, H. and H. Schmidt: Ozone episode analysis by four dimensional variational chemistry data assimilation, J. Geophys. Res., 106(D4), 3569–3590, 2001.

Eller, P., Singh, K., Sandu, A., Bowman, K. W., Henze, D. K. and Lee, M.: Implementation and evaluation of an array of chemical solvers in a global chemical transport model, Geophysical Model Development, Vol. 2, p. 1–7, 2009.

Errera, Q. and Fonteyn, D.: Four-dimensional variational chemical assimilation of CRISTA stratospheric measurements, J. Geophys. Res., 106, 12,253-12,265, 2001.

Evensen, G.: Sequential data assimilation with a nonlinear quasi-geostrophic model using Monte Carlo methods to forecast error statistics, J. Geophys. Res, 99, 10143–10162, 1994.

Fisher, M. and Lary, D. J.: Lagrangian four-dimensional variational data assimilation of chemical species, Q. J. R. Meteorol. Soc., 131, 1681-1704, 1995.

Geer, A. J., et al.:The ASSET intercomparison of ozone analyses: Method and first results, Atmos. Chem. Phys., 6, 5445-5474, 2006.

Gaspari, G., Cohn, S. E.: Construction of correlation functions in two and three dimensions, Quarterly Journal of the Royal Meteorological Society, Vol. 125 Issue 554,723-757, 1999.

Gauthier, P., Charette, C., Fillion, L., Koclas, P. and Laroche, S.: Implementation of a 3D Variational Data Assimilation System at the Canadian Meteorological Centre. Part I: The Global Analysis, Atmosphere-Ocean, 37 (2), 103-156, 1999.

Hakami, A., Henze, D. K., Seinfeld, J. H., Chai, T., Tang, Y., Carmichael, G.R. and Sandu, A.: Adjoint inverse modeling of black carbon during ACE-Asia, Journal of Geophysical Research, Vol. 110, D14301, doi:10.1029/2004JD005671, 25 pages, 2005.

Hakami A., Henze D.K., Seinfeld J.H., et al.: The adjoint of CMAQ. Environmental Science and Technology, 41(22):7807–7817, 2007.

Hamer, P., Bowman, K., Henze D., :Observing requirements for geostationary satellites to enable ozone air quality prediction, Atmos. Chem. Phys., *submitted*

Henze D.K., Seinfeld J.H., Liao W., Sandu A., et al.: Inverse modeling of aerosol dynamics: Condensational growth . Journal of Geophysical Research-Atmospheres, Volume: 109, Issue: D14, Article Number: D14201, 2004.

Henze, D. K., Hakami, A. and Seinfeld, J. H.: Development of the adjoint of GEOS-Chem, Atmos. Chem. Phys., 7, 2413-2433, 2007.

Henze, D. K., Seinfeld, J. H. and Shindell, D. T.: Inverse modeling and mapping U.S. air quality influences of inorganic PM2.5 precursor emissions with the adjoint of GEOS-Chem, Atmos. Chem. Phys., 9, 5877-5903, 2009.

Horowitz, L. W., et al.: A global simulation of tropospheric ozone and related tracers: Description and evaluation of MOZART, version 2, J. Geophys. Res., 108(D24), 4784, doi:10.1029/2002JD002853, 2003.

Horowitz, L. W.: Past, present and future concentrations of tropospheric ozone and aerosols: Methodology, ozone evaluation, and sensitivity to aerosol wet removal, J.

Geophys. Res., 111, D22211, doi:10.1029/2005JD006937, 2006.

Houtekamer, P. L., Mitchell, H. L., Pellerin, G., Buehner, M., Charron, M., Spacek, L., and Hansen, B.: Atmospheric Data Assimilation with an Ensemble Kalman Filter: Results with Real Observations, Monthly Weather Review, 133(3):604-620, 2005.

Hudman, R. C., et al.: Surface and lightning sources of nitrogen oxides over the United States: Magnitudes, chemical evolution and outflow, J. Geophys. Res., 112, D12S05, doi:10.1029/2006JD007912, 2007.

Jacob, D.J. Introduction to Atmospheric Chemistry. Princeton University Press, New Jersey, 1999.

Jones, D. B. A., Bowman, K. W., Logan, J. A., Heald, C. L., Liu, J., Luo, M., Worden, J. and Drummond, J.: Inversion analysis of carbon monoxide emissions using data from the TES and MOPITT satellite instruments, Atmospheric Chemistry and Physics Discussions,7,6, 17625–17662, 2007.

Jones, D. B. A., Bowman, K. W., Palmer, P. I., Worden, J. R., Jacob, D. J., Hoffman, R. N., Bey, I. and Yantosca, R. M.: Potential of observations from the Tropospheric Emission Spectrometer to constrain continental sources of carbon monoxide, J. Geophys. Res., 108, (D24), 2003.

Kalnay, E.: Atmospheric modeling, data assimilation and predictability, Cambridge University Press, 2002.

Khattatov, B. V., Gille, J. C., Lyjak, L. V., Brasseur, G. P., Dvortsov, V. L., Roche, A. E. and Walters, J.: Assimilation of photochemically active species and a case analysis of UARS data, Journal of Geophysical Research, 104:18715–18737, 1999.

Khattatov, B. V., Lamarque, J. -F., Lyjak, L. V., Menard, R., Levelt, P., Tie, X., Brasseur, G. P. and Gille, J. C.: Assimilation of satellite observations of long-lived chemical species in global chemistry transport models, J. Geophys. Res., 105(D23), 29–135, 2000.

Kopacz, M., Jacob, D. J., Henze, D. K., Heald, C. L., Streets, D. G., and Zhang, Q.: A comparison of analytical and adjoint Bayesian inversion methods for constraining Asian sources of CO using satellite (MOPITT) measurements of CO columns, Journal of Geophysical Research, 2007, 114, D04305.

Lahoz, W. A., et al.: The Assimilation of Envisat data (ASSET) project, Atmos. Chem. Phys., 7, 1773-1796, 2007.

Lahoz, W. and Errera, Q.: Constituent Assimilation, in: Data Assimilation: Making sense of observations, edited by Lahoz, W., Kahattatov, B., and Ménard, R., pp. 449 -490, Springer, 2010.

Lamarque, J.-F., Khattatov, B. V. and Gille, J. C.: Constraining tropospheric ozone column through data assimilation, J. Geophys. Res., 107(D22), 4651, doi:10.1029/2001JD001249, 2002.

Laroche, S., Dorval, E. C., Canada, Q. C., Gauthier, P., Tanguay, M., Pellerin, S., and Morneau, J.: Evaluation of the operational 4D-Var at the Meteorological Service of Canada, 21st Conference on Weather Analysis and Forecasting, 14B.3, 2005.

LeDimet, F.-X. and Talagrand, O.: Variational algorithms for analysis and assimilation of meteorological observations: theoretical aspects, Tellus 38A, 97-110, 1986.

Li, Z. and Navon, I. M.: Optimality of variational data assimilation and its relationship with the Kalman filter and smoother, Q. J. R. Meteorol. Soc., 127, pp. 661-683, 2001.

Li, Q., Jacob, D. J., Park, R. J., Wang, Y., Heald, C. L., Hudman, R. C., Yantosca, R. M., Martin, R. V., and Evans, M. J.: North American pollution outflow and the trapping of convectively lifted pollution by upper-level anticyclone, J. Geophys. Res., 110, D10301, doi:10.1029/2004JD005039, 2005.

Liao WY, Sandu A, Carmichael GR, et al.: Singular vector analysis for atmospheric chemical transport models, Monthly Weather Review, 134(9):2443–2465, 2006.

Lions, J. L.: Optimal control of systems governed by partial differential equations, Springer-Verlag, 1971.

Logan, J. A.: Trends in the vertical distribution of ozone: An analysis of ozonesonde data, J. Geophys. Res., 99(D12), 25,553-0–25,585, 1994.

Logan, J. A.: An analysis of ozonesonde data for the troposphere: Recommendations for testing 3-D models and development of a gridded climatology for tropospheric ozone, J. Geophys. Res., 104(D13), 16,115-16,149, 1999.

McLinden, C. A., Olsen, S. C., Hannegan, B., Wild, O., Prather, M. J., and Sundet, J.: Stratospheric ozone in 3-D models: A simple chemistry and the cross-tropopause flux, J. Geophys. Res., 105(D11), 14,653-14,665, doi:10.1029/2000JD900124, 2000.

Menard, R., Cohn, S. E., Chang, L. -P. and Lyster, P. M.: Assimilation of stratospheric chemical tracer observations using a Kalman Filter I: Formulation, Mon. Weather Rev., 128, 2654-2671, 2000.

Munro, R., Siddans, R., Reburn, W. J., and Kerridge, B. J.: Direct measurement of tropospheric ozone distributions from space, Nature, 392(6672), 168-171, 1998.

Nassar, R., Logan, J. A., Worden, H. M., et al.: Validation of Tropospheric Emission Spectrometer (TES) nadir ozone profiles using ozonesonde measurements,J. Geo-

phys. Res., 113, D15S17, doi:10.1029/2007JD008819, 2008.

Navon, I. M.: Data assimilation for Numerical Weather Prediction: a review, in: Data Assimilation for Atmospheric, Oceanic, and Hydrologic Applications, XVIII, 475 p. 326 illus., Hardcover, ISBN: 978-3-540-71055-4, 2009.

Oltmans, S. J., et al.: Long-term changes in tropospheric ozone, Atmos. Environ., 40, 3156-3173, 2006.

Ott, E., Hunt, B. R., Szunyogh, I., Zimin, A.V., Kostelich, E. J., Kostelich, M., Corazza, M., Sauer, T., Kalnay, E., Patil, D. J. and Yorke, J. A: A local ensemble Kalman Filter for Atmospheric Data Assimilation, Tellus, Vol. 56A, pp. 415-428, 2004.

Palmer, P. I., Jacob, D. J., Jones, D. B. A., Heald, C. L., Yantosca, R. M., Logan, J. A., Sachse, G. W. and Streets, D. G.: Observations over the western Pacific, 2003.

Parrington, M., Jones, D. B. A., Bowman, K. W., Horowitz, L. W., Thompson, A. M., Tarasick, D. W. and Witte, J. C.: Estimating the summertime tropospheric ozone distribution over North America through assimilation of observations from the Tropospheric Emission Spectrometer, Journal of Geophysical Research, Vol 113, D18307, doi:10.1029/2007JD009341, 2008.

Parrington, M., Jones, D. B. A., Bowman, K. W., Thompson, A. M., Tarasick, D. W., Merrill, J., Oltmans, S. J., Leblanc, T., Witte, J. C. and Millet, D. B.: Impact of the assimilation of ozone from the tropospheric emission spectrometer on surface ozone across North America, Geophysical Research Letters 36 (4), 2009.

Parrish, D. F. and Derber, J. C.: The national meteorological center's spectral statistical-interpolation analysis system, Monthly Weather Review, (120), p. 1747–1763, 1992.

Pierce, R. B., et al.: Chemical data assimilation estimates of continental U. S. ozone and nitrogen budgets during the Intercontinental Chemical Transport Experiment-North America, J. Geophys. Res., 112, D12S21, doi:10.1029/2006JD007722, 2007.

R. B. Pierce, J. Al-Saadi, C. Kittaka, T. Schaack, A. Lenzen, K. Bowman, J. Szykman, A. Soja, T. Ryerson, A. M. Thompson, P. Bhartia, and G. A. Morris. Impacts of background ozone production on Houston and Dallas, Texas, air quality during the Second Texas Air Quality Study field mission. J. Geophys. Res., 114, 05 2009.

Pires, C., Vautard, R., and Talagrand, O.: On extending the limits of variational assimilation in nonlinear chaotic systems, Tellus, 48A, 960-121, 1996.

Price, C., and Rind, D.: A Simple Lightning Parameterization for Calculating Global Lightning Distributions, J. Geophys. Res., 97(D9), 9919-9933, doi:10.1029/92JD00719, 1992.

Rabier, F., Jarvinen, H., Klinker, E., Mahfouf, J. -F. and Simmons, A.: The ECMWF operational implementation of four-dimensional variational data assimilation I: Experimental results with simplified physics, Quarterly Journal of the Royal Meteorological Society, 126:1143–1170, 2000.

Sandu, A., Daescu, D., and Carmichael, G.R.: Direct and Adjoint Sensitivity Analysis of Chemical Kinetic Systems with KPP: I - Theory and Software Tools, Atmos. Environ., 37(36):5083-5096, 2003.

Daescu D.N., Sandu A., Carmichael G.R.: Direct and adjoint sensitivity analysis of chemical kinetic systems with KPP: II - Numerical validation and applications, Atmos. Environ., 37(36):5097–5114, 2003.

Sandu, A., Daescu, D. N., Carmichael, G. R. and Chai, T.: Adjoint sensitivity analysis of regional air quality models, Journal of Computational Physics, Vol. 204, p. 222–252, 2005.

Sandu A., Liao W., Carmichael G.R., et al.: Inverse modeling of aerosol dynamics using adjoints: Theoretical and numerical considerations, Aerosol science and Technology, 39(8):677–694, 2005.

Sandu A. and Zhang L.: Discrete second order adjoints in atmospheric chemical transport modeling, Journal of Computational Physics, 227 (12), 5949–5983, 2008.

Sasaki, Y. K.: An objective analysis based on the variational method, J. Met. Soc. Jap. II(36), 77–88, 1958.

Segers, A. J., Eskes, H. J., van der A, R. J., van Oss, R. F. and van Velthoven, P. F. J.: Assimilation of GOME ozone profiles and a global chemistry-transport model, using a Kalman Filter with anisotropic covariance, Quarterly Journal of the Royal Meteorological Society, 131, 477-502, 2005.

Singh, K., Eller, P., Sandu, A., Bowman, K. W., Jones, D. B. A. and Lee, M.: Improving GEOS-Chem model forecasts through profile retrievals from Tropospheric Emission Spectrometer, in: Lecture Notes on Computational Science vol. 5545, p. 302–311, International Conference on Computational Science 2009, Baton Rouge, Louisiana, May 25–27, 2009.

Singh, K., Eller, P., Sandu, A., Henze, D., Bowman, K. W., Kopacz, M. and Lee, M.: Towards the construction of a standard adjoint GEOS-Chem model, High Performance Computing Symposium (HPC 2009) at Spring Simulation Multiconference (SpringSim'09), San Diego, California, March 22–27, 2009.

Singh, K., Jardak, M., Sandu, A., Bowman, K. W., Jones, D. B. A., Lee, M.: Construction of non-diagonal background error covariance matrices in global chemical data assimilation, Geophysical Model Development, 4, 299-316, doi:10.5194/gmd-4-299-2011, 2011.

Singh, K., Sandu, A., Jardak, M., Bowman, K. W., Lee, M.: A Practical Method to Estimate Information Content in the Context of 4D-VAR Data Assimilation, *to be submitted to* Journal of Geophysical Research, 2011.

Singh, K., Sandu, A.: Variational Chemical Data Assimilation with Approximate Adjoints, *accepted in* Computers & Geosciences-Elsevier, 2011.

Stevenson, D. S., et al.: Multimodel ensemble simulations of present-day and near-future tropospheric ozone, J. Geophys. Res., 111, D08301, doi:10.1029/2005JD006338, 2006.

Tang YH, Carmichael GR, Horowitz LW, A. Sandu, et. al: Multiscale simulations of tropospheric chemistry in the Eastern Pacific and on the US West Coast during spring 2002 Journal of Geophysical Research-Atmospheres, Volume: 109, Issue: D23, Article Number: D23S11, 2004.

Tarasick, D. W., Fioletov, V. E., Wardle, D. I., Kerr, J. B., and Davies, J.: Changes in the vertical distribution of ozone over Canada from ozonesondes: 1980-2001, J. Geophys. Res., 110, D02304, doi:10.1029/2004JD004643, 2005.

Tellmann, S., Rozanov, V. V., Weber, M., and Burrows, J. P.: Improvements in the tropical ozone profile retrieval from GOME-UV/Vis nadir spectra, Adv. Space Res., 34(4), 739-743, 2004.

TES Science Team, TES L2 Data Users Guide, Jet Propulsion Laboratory, California Institute of Technology, Pasadena, California. (Available at http://tes.jpl.nasa.gov/docsLinks/DOCUMENTS/TESL2DataUsersGuidev2.0.pdf), 2006.

Thompson, A. M., et al.(2007a): Intercontinental chemical transport experiment ozonesonde network study (IONS) 2004: 1. Summertime upper troposphere/lower stratosphere ozone over northeastern North America, J. Geophys. Res., 112 D12S12, doi:10.1029/2006JD007441, 2007. Thompson, A. M., et al.(2007b): Intercontinental chemical transport experiment ozonesonde network study (IONS) 2004: 2. Tropospheric ozone budgets and variability over northeastern North America, J. Geophys. Res., 112 D12S13, doi:10.1029/2004JD005359, 2007.

Todling, R., Cohn, S. E.: Suboptimal Schemes for Atmospheric Data Assimilation Based on the Kalman Filter, Monthly Weather Review, 122, 2530-2557, 1994.

Worden, J. R., Bowman, K. W. and Jones, D. B. A.: Characterization of atmospheric profile retrievals from Limb Sounding Observations of an inhomogeneous atmosphere, J. Quant. Spectrosc. Radiat. Transfer, 86, (03)00274-7, 2004.

Wu, L., Mallet, V., Bocquet, M. and Sportisse, B.: A comparison study of data assimilation algorithms for ozone forecasts, J. Geophys. Res., 113, D20310, 2008.

Yevich, R., and Logan, J. A.: An assessment of biofuel use and burning of agricultural waste in the developing world, Global Biogeochem. Cycles, 17(4), 1095, doi:10.1029/2002GB001952, 2003.

Zhang, L., Constantinescu, E. M., Sandu, A., Tang, Y., Chai, T., Carmichael, G. R., Byun, D., Olaguer, E.: An adjoint sensitivity analysis and 4D-Var data assimilation study of Texas air quality, Atmospheric Environment, Vol. 42, Issue 23, p. 5787–5804,

2008.

Zhang, L., Jacob, D. J., Kopacz, M., Henze, D. K., Singh, K., and Jaffe, D. A.: Intercontinental source attribution of ozone pollution at western U.S. sites using an adjoint method, Geophys. Res. Lett., 36, L11810, doi:10.1029/2009GL037950, 2009.

Zhu, C., Byrd, R. H. and Nocedal, J.: L-BFGS-B: Algorithm 778: L-BFGS-B, FORTRAN routines for large scale bound constrained optimization, ACM Transactions on Mathematical Software, Vol 23, Num. 4, pp. 550 - 560, 1997.

Appendix A: The 3D-Var equivalent initial condition

Finally, we want to determine the "3D-Var equivalent initial condition" $\mathbf{x}_0^{e(3)}$ such that the resulting trajectory fits best the 3D-Var analysis in a least squares sense. To our knowledge, no attempt has been made to date to estimate the equivalent effect of all 3D-Var corrections at the initial time. (Note that the 3D-Var analysis is not a trajectory of the model). The dynamic equations for the 3D-Var trajectory, linearized about the 4D-Var analysis, read:

$$\mathbf{x}_i^{a(3)} - \mathbf{x}_i^{a(4)} = \mathbf{M}_i \cdot \left(\mathbf{x}_0^{e(3)} - \mathbf{x}_0^{a(4)} \right) + \theta_i \,, \quad i = 0, \cdots, N \,. \tag{A1}$$

The errors $\theta_i = \mathbf{x}_i^{a(3)} - \mathbf{x}_i^{e(3)}$ are assumed to be normally distributed with mean zero and covariance $\mathbf{Q}_i$. We now seek the equivalent 3D-Var initial condition that solves (A1) in a least squares sense. The scaled linearized dynamic equations are

$$\mathbf{Q}_i^{-1/2} \mathbf{M}_i \left(\mathbf{x}_0^{e(3)} - \mathbf{x}_0^{a(4)} \right) - \mathbf{Q}_i^{-1/2} \left(\mathbf{x}_i^{a(3)} - \mathbf{x}_i^{a(4)} \right) = \mathbf{Q}_i^{-1/2} \theta_i \,, \quad i = 0, \cdots, N \,,$$

and involve the scaled residuals $\mathbf{Q}_i^{-1/2} \theta_i$ which are standard normal random vectors. Therefore the least squares solution is the one that minimizes the sum of scaled

residual norms squared

$$\mathbf{x}_0^{e(3)} = \arg\min \sum_{i=0}^{N} \left\| \mathbf{M}_i \left(\mathbf{x}_0^{e(3)} - \mathbf{x}_0^{a(4)} \right) - \left(\mathbf{x}_i^{a(3)} - \mathbf{x}_i^{a(4)} \right) \right\|^2_{\mathbf{Q}_i^{-1}} .$$

The minimum of this quadratic function is obtained by imposing that its gradient equals zero. This leads to the following system of linear equations:

$$\underbrace{\left(\sum_{i=0}^{N} \mathbf{M}_i^T \, \mathbf{Q}_i^{-1} \, \mathbf{M}_i \right)}_{\nabla^2_{\mathbf{x}_0^a, \mathbf{x}_0^a} \mathcal{D}\left(\mathbf{x}_0^{a(4)}\right)} \left(\mathbf{x}_0^{e(3)} - \mathbf{x}_0^{a(4)} \right) = \underbrace{\sum_{i=0}^{N} \mathbf{M}_i^T \, \mathbf{Q}_i^{-1} \, \left(\mathbf{x}_i^{a(3)} - \mathbf{x}_i^{a(4)} \right)}_{\nabla_{\mathbf{x}_0^a} \mathcal{D}\left(\mathbf{x}_0^{a(4)}\right)} .$$

Therefore the least squares solution to finding the 3D-Var equivalent initial condition is

$$\mathbf{x}_0^{e(3)} = \mathbf{x}_0^{a(4)} - \left(\nabla^2_{\mathbf{x}_0^a, \mathbf{x}_0^a} \mathcal{D} \left(\mathbf{x}_0^{a(4)} \right) \right)^{-1} \cdot \nabla_{\mathbf{x}_0^a} \mathcal{D} \left(\mathbf{x}_0^{a(4)} \right) . \tag{A2}$$

Consider a standard normal random perturbation is applied at t_0 to the 4D-Var optimal initial condition. This perturbation is propagated through the linearized model, and its covariance at t_i is $\mathbf{M}_i \mathbf{M}_i^T$. Let $\mathbf{Q}_i = \rho_i \, \mathbf{M}_i \mathbf{M}_i^T$ in (23) in order to account for an increasing error with the model evolution. The scalar weights ρ_i decrease with i, to account for the reduction in uncertainty through 3D-Var assimilation, and are chosen such that $\sum_{i=0}^{N} \rho_i = 1$. Using the fact that $\mathbf{M}_i^T \, \mathbf{Q}_i^{-1} \, \mathbf{M}_i = \mathbb{I}$ for all i we have that the equivalent 3D-Var initial solution is

$$\mathbf{x}_0^{e(3)} = \mathbf{x}_0^{a(4)} - \sum_{k=0}^{N} \mathbf{M}_i^T \, \mathbf{Q}_i^{-1} \, \left(\mathbf{x}_0^{a(4)} - \mathbf{x}_0^{a(3)} \right) = \mathbf{x}_0^{a(4)} - \nabla_{\mathbf{x}_0^a} \mathcal{D} \left(\mathbf{x}_0^{a(4)} \right) .$$

The 3D-Var solution has incorporated all the observation information when it reaches t_N, the end of the assimilation window. Therefore it makes sense to choose $\rho_0 = \cdots = \rho_{N-1} = 0$ and $\rho_N = 1$ in order to have the equivalent initial condition match the 3D-Var analysis only at the final time. In this case

$$\mathbf{x}_0^{e(3)} = \mathbf{x}_0^{a(4)} - \left(\mathbf{M}_N^T \, \mathbf{Q}_N^{-1} \, \mathbf{M}_N \right)^{-1} \, \mathbf{M}_N^T \, \mathbf{Q}_N^{-1} \, \left(\mathbf{x}_0^{a(4)} - \mathbf{x}_0^{a(3)} \right) . \tag{A3}$$

Table 1. Timing results for GEOS-Chem free model runs using SMVGEAR and KPP chemistry, suboptimal Kalman filter, 3D-Var and 4D-Var data assimilations with diagonal background error covariance matrix for a 24 hour simulation starting 00:00 GMT August 1, 2006.

Experiment Description	CPU Time
Free model run, SMVGEAR chemistry solver	2 min 50 sec
Free model run, KPP chemistry solver	3 min 18 sec
Suboptimal Kalman filter with diagonal $\mathbf{P}^f$	3 min 08 sec
3D-Var with diagonal $\mathbf{B}$	3 min 57 sec
4D-Var with diagonal $\mathbf{B}$ (per model run)	16 min 51 sec

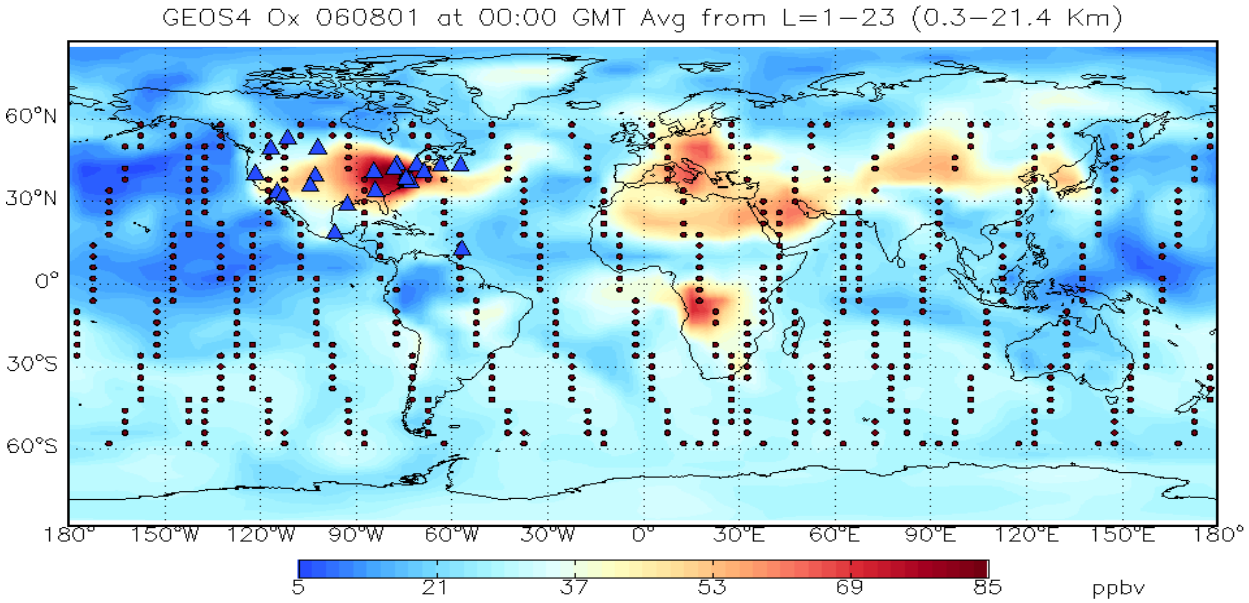

Figure 1. Ozonesonde sounding stations (triangles) used during IONS06 campaign and AURA/TES satellite trajectory snapshots (dots) plotted over the global ozone distribution on August 1st, 2006.

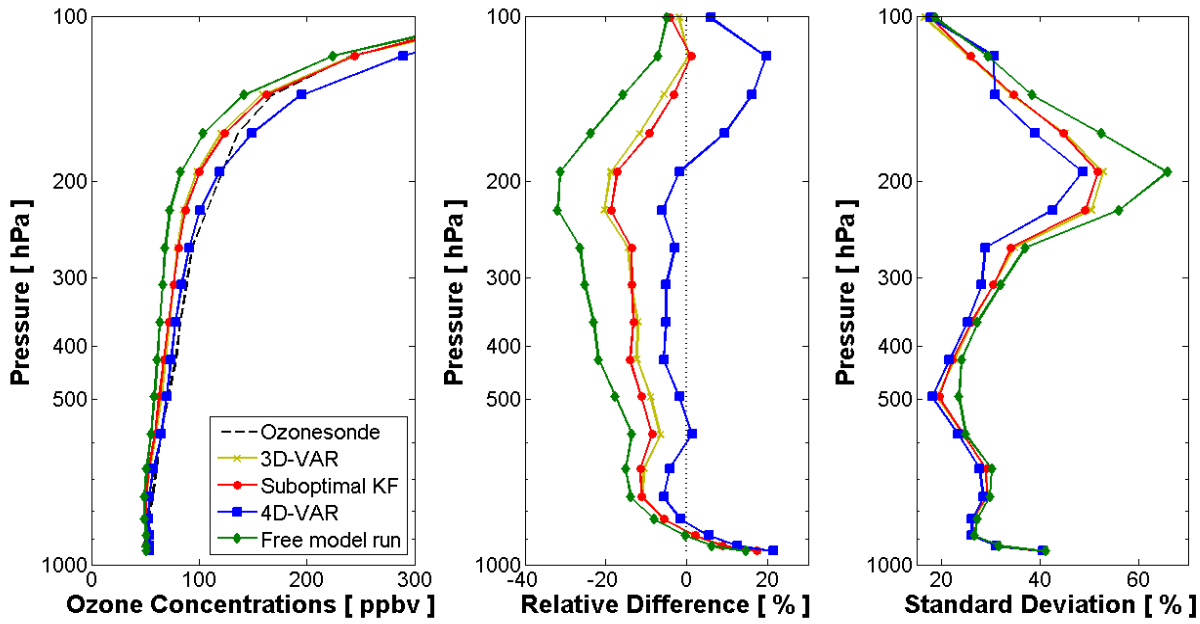

Figure 2. The impact of ozone profile retrievals from TES on data assimilation systems for GEOS-Chem. Left panel: mean ozone concentrations sampled at ozonesonde locations and times for 3D-Var, 4D-Var, suboptimal KF analyses and free model trajectories. Center panel: relative mean errors of predicted ozone concentrations with respect to ozonesonde measurements. Right panel: standard deviation of absolute values of errors with respect to ozonesonde measurements. The data is averaged over all ozonesonde launches. These plots were generated from 5 days simulation from 00:00 GMT August 1, 2006 to 00:00 GMT August 6, 2006 and compared against ozonesonde data available for the month of August.

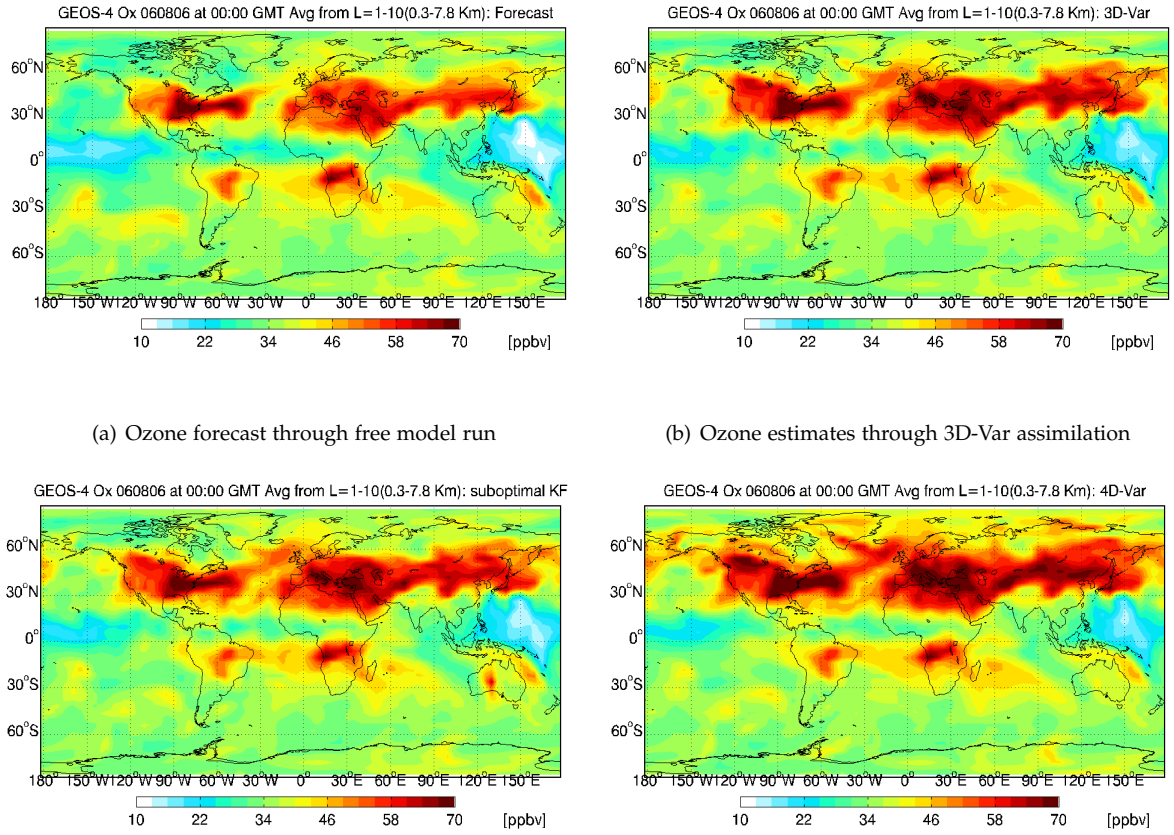

(a) Ozone forecast through free model run

(b) Ozone estimates through 3D-Var assimilation

(c) Ozone estimates through suboptimal Kalman filter

(d) Ozone estimates through 4D-Var assimilation

Figure 3. Global ozone distribution at 00:00 GMT on August 6, 2006 averaged over the first 10 GEOS-Chem vertical levels. Panels (a)-(d): Global tropospheric ozone estimates provided by free model run and suboptimal KF, 3D-Var, and 4D-Var data assimilation systems from a 5-day simulation.

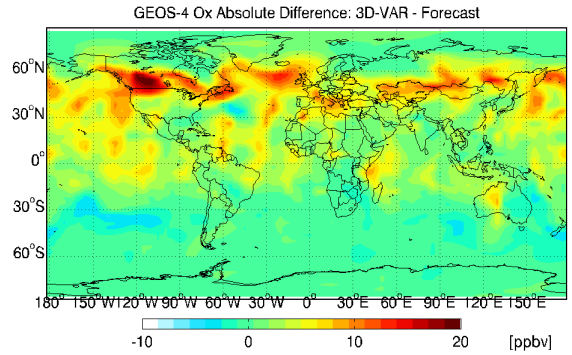

(a) Absolute difference between 3D-Var analysis and the free model run

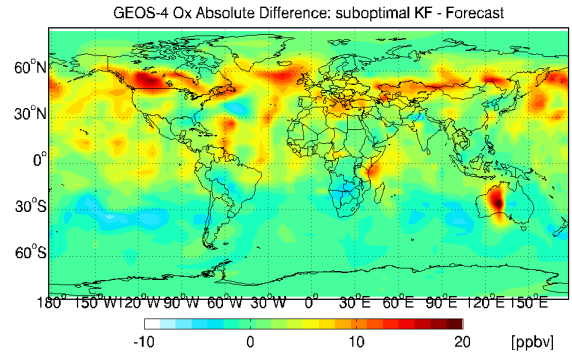

(b) Absolute difference between suboptimal Kalman filter analysis and the free model run

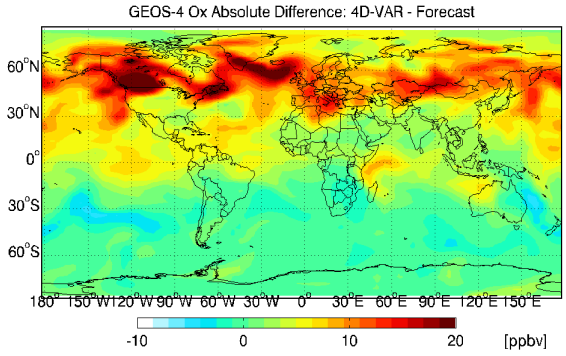

(c) Absolute difference between 4D-Var analysis and the free model run

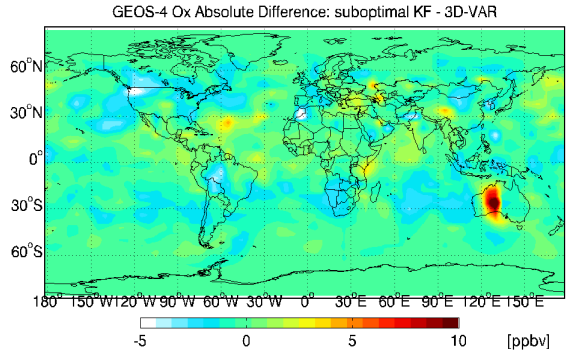

(d) Absolute difference between suboptimal Kalman filter and the 3D-Var analyses

Figure 4. Differences in global ozone concentrations at 00:00 GMT on August 6, 2006, the end of 5-day simulation, averaged over first 10 GEOS-Chem vertical levels. Panels (a)-(c): Differences between suboptimal KF, 3D-Var, and 4D-Var analysis fields and the model forecast (solution without data assimilation). Panel (d): Difference between suboptimal KF and 3D-Var analysis fields.

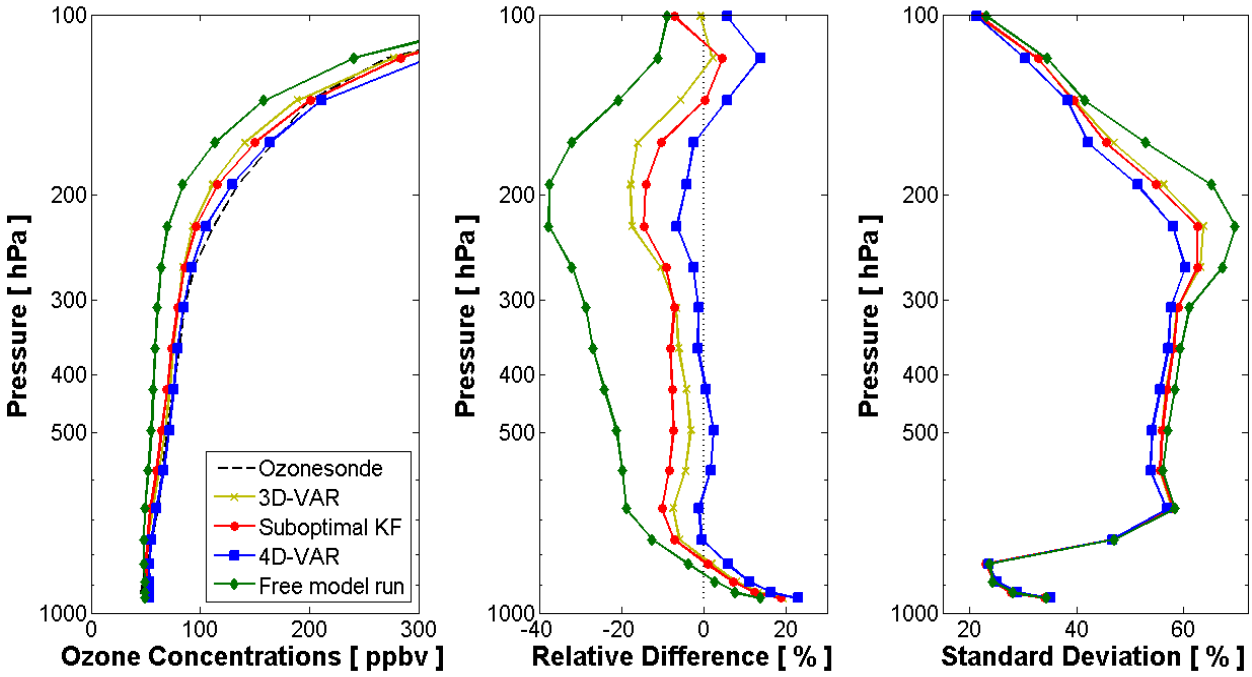

Figure 5. The impact of ozone profile retrievals from TES on data assimilation systems for GEOS-Chem. Left panel: mean ozone concentrations at ozonesonde locations for 3D-Var, 4D-Var, suboptimal KF analyses and free model trajectories. Center panel: relative mean errors of predicted ozone concentrations with respect to ozonesonde measurements. Right panel: standard deviation of absolute values of errors with respect to ozonesonde measurements. The data is averaged over all ozonesonde launches. These plots were generated from 2 weeks simulation from 00:00 GMT August 1, 2006 to 00:00 GMT August 15, 2006 and compared against ozonesonde data available for the month of August.

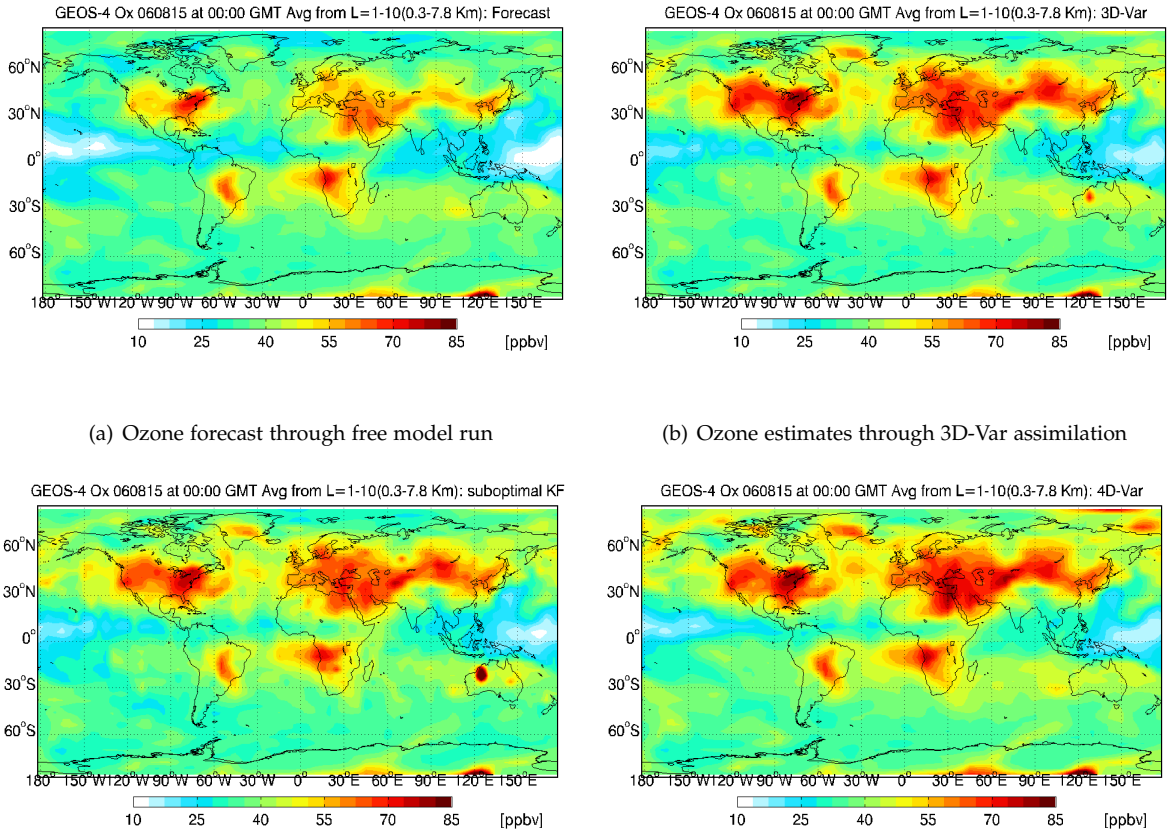

(a) Ozone forecast through free model run

(b) Ozone estimates through 3D-Var assimilation

(c) Ozone estimates through suboptimal Kalman filter

(d) Ozone estimates through 4D-Var assimilation

Figure 6. Global ozone distribution at 00:00 GMT on August 15, 2006 averaged over the first 10 GEOS-Chem vertical levels. Panels (a)-(d): Global tropospheric ozone estimates provided by free model run and suboptimal KF, 3D-Var, and 4D-Var data assimilation systems from a 2-week simulation.

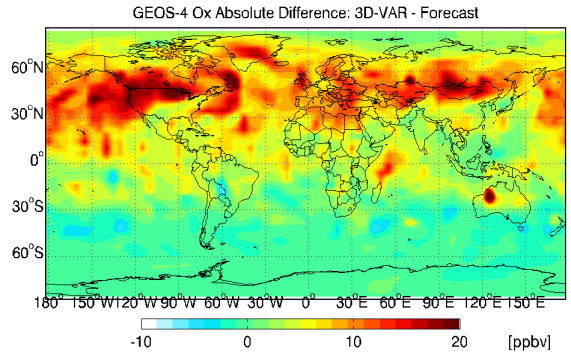

(a) Absolute difference between 3D-Var analysis and the free model run

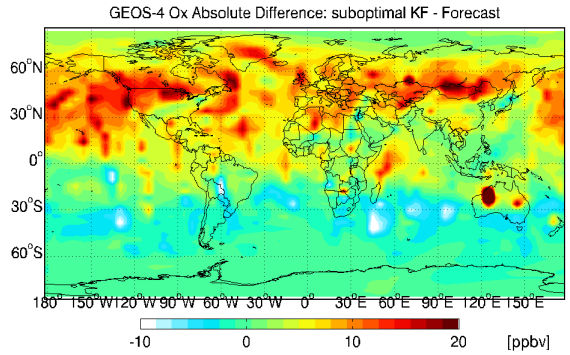

(b) Absolute difference between suboptimal Kalman filter analysis and the free model run

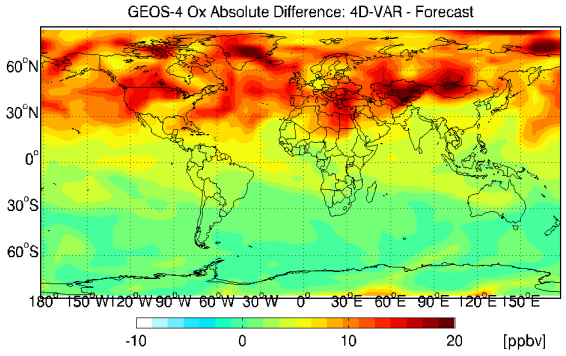

(c) Absolute difference between 4D-Var analysis and the free model run

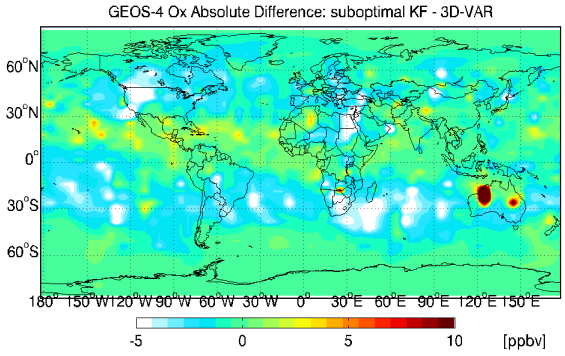

(d) Absolute difference between suboptimal Kalman filter and the 3D-Var analyses

Figure 7. Differences in global ozone concentrations at 00:00 GMT on August 15, 2006, the end of 2-week simulation, averaged over first 10 GEOS-Chem vertical levels. Panels (a)-(c): Differences between suboptimal KF, 3D-Var, and 4D-Var analysis fields and the model forecast (solution without data assimilation). Panel (d): Difference between suboptimal KF and 3D-Var analysis fields.

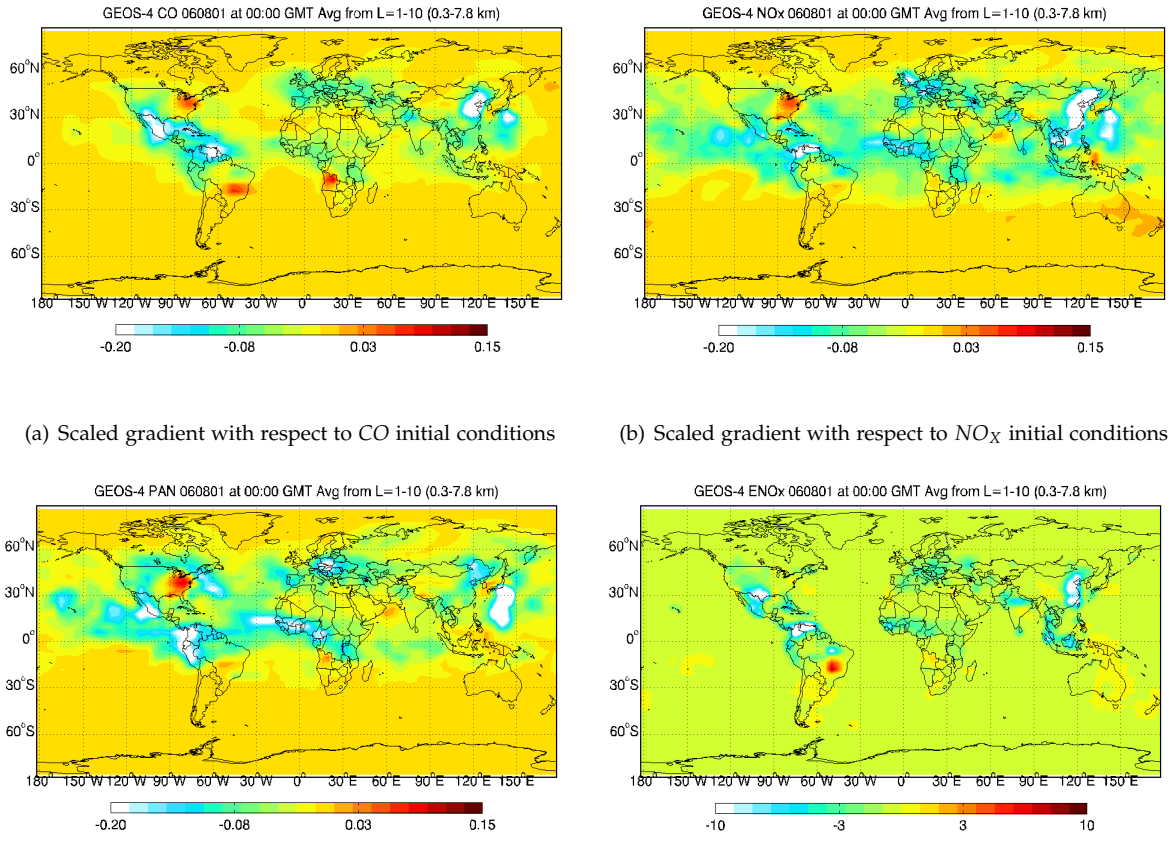

(a) Scaled gradient with respect to *CO* initial conditions

(b) Scaled gradient with respect to NO_X initial conditions

(c) Scaled gradient with respect to *PAN* initial conditions

(d) Scaled gradient with respect to NO_X emissions

Figure 8. Scaled adjoint sensitivities of the 4D-Var cost function (9) with respect to different model parameters. The calculations correspond to the optimal initial ozone concentration. The 4D-Var cost function involves differences between simulated and observed O_X. Panels (a),(b),(c) show sensitivities with respect to initial conditions of other chemical species (at 00:00 GMT on August 1, 2006). The sensitivities with respect to NO_X emissions in panel (d) correspond to emissions over the entire two-week assimilation window. All scaled sensitivity fields are averaged over the first 10 GEOS-Chem vertical levels.

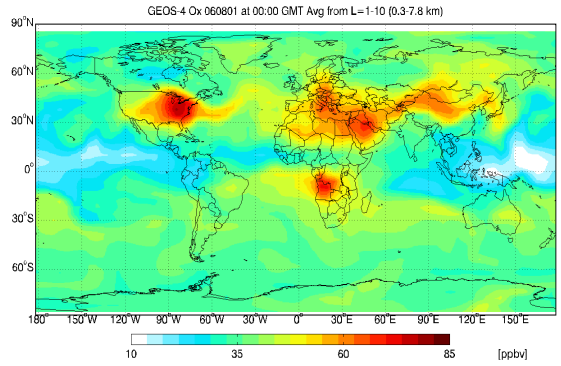

(a) Free model ozone concentration at the beginning of the assimilation window

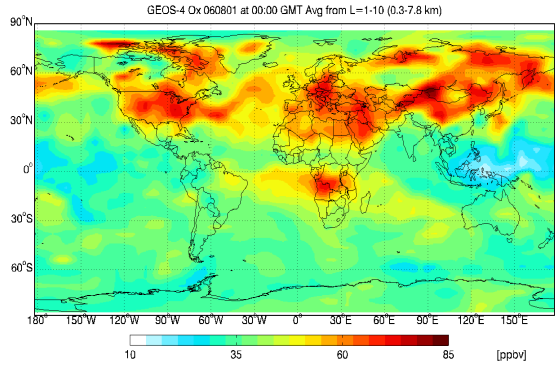

(b) 4D-Var ozone analysis at the beginning of the assimilation window

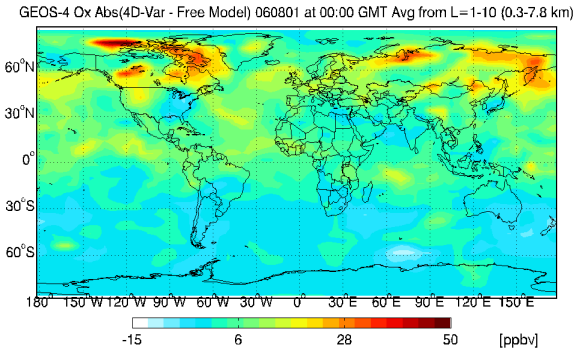

(c) Absolute difference between the 4D-Var optimal initial condition, and the background initial condition

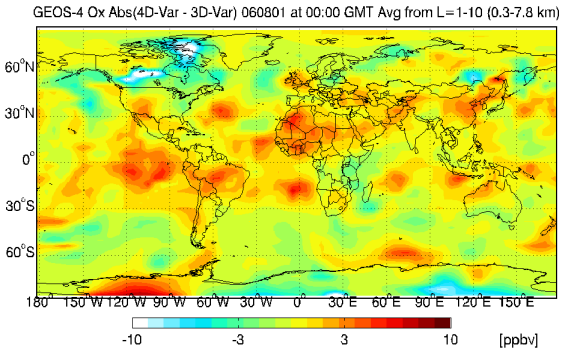

(d) Cumulative difference between the 4D-Var and 3D-Var analyses throughout the assimilation window

Figure 9. The cumulative difference (25) between the 4D-Var and the 3D-Var ozone analyses, projected at the beginning of the five days assimilation window, and averaged over the first 10 GEOS-Chem vertical levels. A two-week long data assimilation window is used, starting at 00:00 GMT on August 1, 2006.